2012

Low-dimensional micro/nanoscale thermal transport

Nathan Van Velson
Iowa State University

Low-dimensional micro/nanoscale thermal transport

by

Nathan Van Velson

A thesis submitted to the graduate faculty

in partial fulfillment of the requirements for the degree of

MASTER OF SCIENCE

Major: Mechanical Engineering

Program of Study Committee:
Xinwei Wang, Major Professor
Terry Meyer
Gap Kim

Iowa State University

Ames, Iowa

2012

Table of Contents

List of Figures

List of Tables

Acknowledgments

First of all, I want to thank my major professor and advisor, Dr. Xinwei Wang. He has been more than just a mentor in the two years that I have spent working for him, he has also been a friend. Dr. Wang has been tremendously supportive and helpful with his insights and advice. I always enjoy our conversations, and I'm sure that I will benefit from my time spent here throughout my career.

I would like to thank the other members of my committee, Dr. Terry Meyer and Dr. Gap Kim. I especially want to thank Dr. Meyer for the opportunity to further broaden my education through an independent study project on bio-oil combustion.

I also want to thank my friends and colleagues who I have worked with in the Micro/Nanoscale Thermal Science Laboratory: Xiaopeng Huang, Yanan Yue, Xiangwen Chen, Xuhui Feng, Guingou Liu, Xiaduan Tang, Jingchao Zhang, Shen Xu, Zaoli Xu, Chong Li, and Huan Lin. I wish the best of luck to all of them in their future endeavors.

I would also like to thank my family, especially my parents, for their support and encouragement, and to all my friends and fellow graduate students in both Lincoln and Ames.

In addition, funding support from the Kansas City Plant and the National Science Foundation is gratefully acknowledged.

Abstract

There is a wide variety of techniques available for characterizing the thermal transport in one-dimensional micro and nanoscale geometries. Two of these techniques have been used extensively to determine the properties of several different samples. The photothermal technique has been used to measure the thermophysical properties of thin films. A transient electrothermal (TET) technique has been used to measure the thermal diffusivity of micro/nanoscale wires and fibers. The TET technique has been modified to measure the thermal contact resistance between two crossed microwires. This contact transient electrothermal (CTET) technique characterizes heat transfer in a single point, essentially zero-dimensional heat transfer. The CTET technique was used to measure the thermal contact resistance between crossed Pt wires and between a glass fiber crossed with a Pt wire.

Chapter 1. Introduction

Micro/nanoscale heat transfer has become an increasingly important field of study in the past two decades. This is due in part to the continual miniaturization of technology, particularly micro/nanoelectronics. It is also partly due to a fundamental interest in the different phenomena that take place at these small scales. As the size of the domain shrinks, many of the assumptions used in analyzing macroscale heat transfer become less valid and thermal transport can behave much differently than in bulk materials.

Two particular geometries of interest in the field of micro and nanoscale heat transfer are thin films and micro/nano wires and fibers. These micro/nanoscale geometries lend themselves to be modeled as one-dimensional systems. There has been a lot of effort in recent years to develop techniques for characterizing the thermal behavior of these one-dimensional systems. In our laboratory, two techniques in particular have been developed: a photothermal technique for thin film characterization, and a transient electrothermal (TET) technique for micro/nanowire measurement. These techniques have been used extensively to successfully measure thermal properties in these systems.

In this work, it will be shown how a technique developed to characterize one-dimensional heat transfer can be modified and used to characterize zero-dimensional heat transfer. Zero-dimensional transport can be thought of as heat transfer through a single point in space. An example of this is thermal contact resistance between two crossed microwires or fibers. While there is a finite contact area, it is small enough compared to the size of the wires to be considered a single point. The heat transfer through this single point can be

considered zero-dimensional heat transfer. There is a thermal resistance at this point, but no thermal capacitance.

A contact transient electrothermal (CTET) technique has been developed based on the TET technique and has been used to measure the thermal contact resistance between several sets of crossed wires and fibers. The values obtained for the thermal contact resistance are reasonable and have good agreement between measurements.

Chapter 2. Literature Review

2.1. Background

Since the first formulation of Fourier's Law in 1822, the study of heat transfer has been central to the development and progression of technology, from the advent of the steam engine and the dawn of the industrial revolution, to today where it continues to be important in the analysis of energy, electronics, and other applications.

Over the past century, it has become apparent that heat transfer can behave very differently at small scales from its behavior in bulk materials. This is due to the fact that as the domain of interest becomes smaller, the characteristic dimensions come closer to being comparable to the mean free path of the energy carriers in the material, be they electrons or phonons. For the dimensions encountered in this work, there may be classical microscale size effects due to the increased effect of boundary scattering, but the continuum assumption is still valid and classical phenomenological heat transfer equations can be used.[1,2]

Two geometries that are of particular interest are thin films and micro/nano wires/fibers. In many cases, heat transfer in these materials can be assumed or approximated to be one-dimensional. This has led to the development of many techniques for determining the heat transfer properties of thin films and micro/nano wires. These techniques include the so-called 3ω technique for thin films and wires,[3-12] photoacoustic and photothermal methods for thin films,[13-16] and various non-contact techniques for thin wires, including the transient electrothermal technique.[17-25]

Another concept in the field of heat transfer that is increasingly important at small scales is the thermal contact resistance between materials at interfaces. Many techniques

have been developed for measuring or predicting thermal contact resistances between two dimensional planar surfaces,[26,27] and they will not be discussed here in depth. Instead, various techniques that have been used to determine the thermal contact resistance between two crossed fibers or wires shall be examined. These techniques include molecular dynamics simulations[28-32] and experimental techniques,[33,34] including a T-type probe technique.[35-38]

Micro/nanoscale heat transfer analysis has many applications, from bio-medical devices to direct energy conversion to microscale manufacturing. As transistors get smaller and smaller, and the amount of computing power continues to grow, thermal management of electronic circuits is an increasingly important application of micro/nanoscale heat transfer concepts and techniques. Another interesting possible application for the work presented in this thesis is the analysis of heat transfer through woven textile materials. Being able to measure the thermal contact resistance between individual fibers could help to better predict the heat transfer in and help in the design of these materials.

2.2. 3ω Technique

One technique that is widely used for characterizing thermal properties of micro/nanoscale materials is the 3ω technique. It is called this because it uses the third harmonic of the voltage signal across a sample to extract information about the sample's properties. In the 3ω technique, a heating current at angular frequency ω is passed through the heating element, which creates a temperature oscillation at frequency 2ω. If the resistance of the element varies linearly with temperature, then the resistance of the sample will also have a small oscillation at frequency 2ω. The product of this resistance oscillation and the oscillating heating current results in a voltage oscillation of frequency 3ω.[3,4]

Cahill was the first to apply this technique in the late 1980s.[3] He pioneered this technique and used it to measure the properties of bulk dielectric materials. To do so, he deposited a thin metal line on the surface of a sample which functioned as both heat source and thermometer. The current at frequency ω was passed through this metal line. The width and thickness of the line are small enough compared to its length and the thickness of the sample to ensure that the heat transfer in the sample is two-dimensional. Solving the heat transfer equation gives an expression for the temperature oscillation of the metal line. The amplitude of the voltage at 3ω is related to the temperature oscillation as $\Delta V_{3\omega} = \frac{1}{2} I_0 \frac{dR}{dT} \Delta T$.[5] If *dR/dT* is known then the thermal conductivity of the bulk material can be fitted to the 3ω voltage measurement.

In Cahill's analysis, it was assumed that the thickness of the sample being measured was greater than the thermal diffusion depth at the frequency of oscillation.[3] The thermal diffusion depth D_ω at angular frequency ω is given by

$$D_w = \sqrt{\frac{2\alpha}{\omega}} \tag{1}$$

where α is the thermal diffusivity. For measuring the properties of thin films, this may not be the case. Kim *et al.* extended this method to the measurement of out of plane thermal properties of thin films by developing a multilayer heat transfer model.[6] This method has been improved over the years by attempts to account for the thickness and width of the heating strip[7] and the thermal capacitance of the sample film.[8] It has recently been used to measure the properties of free standing films[9] and thermoelectric materials.[10]

The 3ω technique has also been developed to measure the thermal properties of micro/nano wires. In this method, the sample itself becomes the heat source and temperature sensor in the measurement. For wires where the thermal diffusion length within one heating period is greater than the diameter, the heat transfer in the wire can be considered one dimensional along the axial direction. Lu *et al.* solved the one dimensional heat transfer equation along the wire and found an expression for the amplitude of the 3ω voltage:[11]

$$V_{3\omega} = \frac{4I^3 LRR'}{\pi^4 kS\sqrt{1+(2\omega\gamma)^2}} \tag{2}$$

Here I and $V_{3\omega}$ are the root mean square values of the current and 3ω voltage, respectively, R' is the temperature gradient of the resistance (dR/dT), k is the thermal conductivity, S is the cross sectional area, and γ is the thermal time constant defined as $\gamma = L^2/\pi^2\alpha$; α is the thermal diffusivity. In the high frequency range, this yields information about the thermal conductivity, while very low frequencies can be used to find the thermal diffusivity of the sample. A range of intermediate frequencies can be used in the measurement and the experimental data fitted to find both properties.[11] This method has been used to measure the thermal properties of a variety of materials including multiwalled carbon nanotubes.[12]

In the above analysis, the heat transfer equation was solved assuming constant temperature boundary conditions at the ends of the wire where they are attached to the base. Hou *et al*. takes into account the heat transfer into the base where the sample is mounted.[4] The one-dimensional heat transfer equation was solved for the wire with heat flux boundary conditions at the ends. The three-dimensional heat transfer equation in spherical coordinates was then solved for the base, using a heat flux boundary condition at the interface between

the wire and base. The full solution to both problems was found by combining them using the boundary conditions at the interface.

2.3. Photothermal and Photoacoustic Methods

Our lab has an extremely versatile and effective photothermal technique for measuring thermal properties of thin films that has its basis in related photothermal and photoacoustic techniques that have been developed over the past few decades.

The principle of the photoacoustic method is that a modulated laser beam is directed onto a sample, causing a periodic heating in the sample. The heating of the sample also causes a periodic heating of the air or other gas directly above the sample. The typical photoacoustic cell consists of a gas filled cell containing the sample and a microphone. The periodic heating of the gas above the sample causes a pressure variation in the gas that can be measured with the microphone. Early efforts were made to model the heat transfer in the sample and gas above the sample and the resulting pressure variation in order to be able to extract information about the sample properties from the measurement.[13]

McGahan and Cole developed a photothermal deflection method for measuring the thermal properties of thin films using a similar concept.[14] In this method a modulated laser beam is used to create thermal waves in the sample and heat the ambient gas above the sample. The temperature gradient in the gas above the sample influences the gas's index of refraction. This allows the temperature gradient to be measured by measuring the deflection of a second laser beam that is passed parallel to the surface of the sample. In this method, the sample may consist of any number of optically absorbing layers on a thermally thick substrate. An exact analytical solution for the deflection of the probe beam was found by first

solving the axisymmetric heat equation in each layer. The heat equation was solved using a Green's function method. Continuity for the temperature and heat flux was enforced between layers at the boundaries. In this way, an exact solution was found for the temperature everywhere in the sample and gas layer above the sample.

The above multilayer model is two dimensional and requires a numerical integration. Hu *et al.* developed a generalized solution for one dimensional heat transfer in a multilayer sample and applied it to a photoacoustic technique for measuring thin film thermophysical properties.[15] The one dimensional assumption is valid when the spot size of the incident beam is much greater than the thermal diffusion length of the sample within one heating period. In this solution, any of the layers can be optically absorbing. In addition, the thermal contact resistance between layers can be considered.

Wang *et al.* modified this technique to develop a photothermal method based on measuring the thermal radiation from the sample surface.[16] When the sample is heated by a modulated laser beam, the temperature of the surface will oscillate, thus the thermal radiation from the surface will oscillate as well. Using the solution developed in reference (15), the phase shift between the thermal radiation from the sample and the incident laser beam can be calculated. The thermophysical properties of interest can then be determined by fitting the measured phase shift over a range of modulation frequencies to the theoretical phase shift. This technique will be explained in more detail in section 4.1. along with results from several measured samples.

2.4. TET Technique

The 3ω technique is effective and widely used for characterizing the heat transfer properties of micro/nano wires, but it has several drawbacks as well. The 3ω method can only be used to measure the properties of electrically conducting wires, and the sample must have a linear *I-V* behavior. In addition, the 3ω technique requires a very long measurement time to record data over a wide range of frequencies. These shortcomings of the 3ω method are addressed by a transient electrothermal (TET) technique developed by Guo *et al.*[17] The TET technique can be used to characterize the properties of electrically conductive, nonconductive, and semiconductive materials. It also has the benefit of incredibly short measurement times, often less than one second, and a higher signal to noise ratio.

In the TET technique, the sample wire or fiber is mounted between two copper electrodes. A step direct current is applied to the sample to induce joule heating. The one-dimensional heat diffusion equation can be solved to find the average temperature rise. This rise in temperature will cause a change in electrical resistance in the sample. The change in resistance can be measured by measuring the voltage evolution of the wire. The properties of the sample can thus be extracted from the measured voltage evolution.

The TET technique has been successfully used to characterize the properties of SWCNT bundles,[17] thin films made from TiO_2 nanofibers,[18] free standing P3HT films,[19] and spider silk,[20] among others. This technique will be explained in more detail in section 4.2., along with results from several measured samples.

2.5. Other Non-contact Techniques

Several other techniques for characterizing the thermophysical properties of micro/nano wires and fibers have been developed in recent years. One is the optical heating and electrical thermal sensing (OHETS) technique.[21] In this technique the sample is suspended between two electrodes. A small direct current is applied to the wire while a modulated laser beam is shined on the sample. This causes periodic heating which causes a periodic change in electrical resistance. This resistance change can be measured by measuring the change in voltage. Solving the heat diffusion equation in the wire for the case of periodic heating caused by the laser shows that the phase shift of the voltage variation relative to the laser can be used to extract information about the properties of the sample.

A technique that is very similar to the TET technique is the transient photo-electro-thermal (TPET) technique.[22] For this method, the sample to be measured is mounted between two electrodes and a small dc is applied to the sample. The sample is irradiated by a step cw laser beam, which causes a transient temperature rise and corresponding resistance change in the sample. The development of the physical model for this technique is identical to that of the TET technique, with the volumetric heating being supplied by the laser rather than electrical heating. As in the TET technique, the thermal diffusivity of the sample can be found by fitting the normalized voltage data to the theoretical temperature rise.

For some samples with very high thermal diffusivities, the rising time of the step heating source may be slow enough to introduce significant errors in the TET or TPET technique.[23] A pulsed laser-assisted thermal relaxation (PLTR) technique was developed to address this.[24] In this technique, the sample is again suspended between two electrodes and a

small dc is fed through the sample. The sample is irradiated by a pulsed nanosecond laser to quickly heat the sample. The sample will then cool back down to a steady state temperature. This temperature decay is dependent on the thermal properties of the sample. This temperature decay is recorded as a voltage decay and can be used to find the properties by fitting the experimental data to a theoretical curve found by solving the 1D heat equation.

Another method was developed for characterizing MWCNT bundles using a steady-state electro-Raman thermal (SERT) technique.[25] The SERT technique also enables direct temperature measurement, which other non-contact methods do not. The principle of the experiment is based on the temperature dependence of the Raman spectrum of CNTs. Both the location and intensity of the peaks in the Raman spectrum of CNTs are temperature dependent and can be used to measure the temperature of a CNT sample. The thermal conductivity of the sample can be determined from a linear fitting of the temperature plotted against heating power.

2.6. Thermal Contact Resistance

At the interface between two materials, there is always a finite temperature drop that is due to what is known as the thermal contact resistance (TCR). The thermal contact resistance at an interface is defined as $R_c = \Delta T / q$ for heat flux in Watts, q and has units of K/W.[39] It can also be normalized as a resistance per unit area and have units of m^2K/W. Sometimes this interfacial thermal resistance can be ignored, but often it cannot. The existence of a TCR at the interface between two materials is due to the roughness of the surfaces which makes the contact non-ideal. Yovanovich has an excellent summary of the

historical development of models to predict the TCR between conforming rough surfaces, including the effects that local mechanical deformation has on the amount of contact area.[26]

Even when the contact between two materials is ideal, there will be a finite temperature drop at the interface. This is due to a difference in the structure and vibrational properties between the materials. This is known as a thermal boundary resistance (TBR). Swartz and Pohl describe an acoustic mismatch model and a diffuse mismatch model to predict the TBR.[27] Assuming perfect contact, in the acoustic mismatch model, phonons incident on the boundary are either transmitted through the boundary or reflected back, with a probability depending only on the phonon equivalent of Snell's law. Alternatively, in the diffuse mismatch model, all incident phonons are diffusely scattered. This allows for more heat transfer and a lower TBR. These two models provide limiting cases for the TBR. For normal solid-solid interfaces at room temperatures, the TCR due to surface roughness has a far larger effect than the TBR. However, for micro and nanoscale materials, the TBR may play a more important role.

There is particular interest in the role that thermal contact resistance plays in micro and nanoscale heat transfer, especially its influence on the heat transfer between crossed wires or fibers. In the next sections, some methods of characterizing the TCR for such contacts are discussed.

2.7. Molecular Dynamics Simulations

Molecular dynamics (MD) simulation is a useful tool for predicting heat transfer in nanoscale systems. Briefly, MD simulations model the motion of individual atoms by solving Newton's laws of motion for each atom. The forces acting on each atom due to the presence

of other atoms are calculated by choosing an appropriate potential function.[1,2] Information about thermal transport can be extracted from the calculated motions of the atoms.

Recently, several MD studies have been done on composite materials containing CNTs. These composite materials had a much lower measured effective thermal conductivity than expected given the high thermal conductivity of individual CNTs.[28] The reason for this was proposed to be the interfacial thermal resistance between the CNTs and the matrix and the resistance between crossed CNTs.[29] MD simulations of CNTs in an octane matrix confirmed that there is a very high thermal boundary resistance between the CNTS and the matrix.[28,29]

MD simulations were also done of crossed CNTs. Zhong *et al*. modeled two SWCNTs in contact and determined the TCR between them by fitting the temperature profiles obtained by the MD simulations to a finite difference solution of the heat equation in the SWCNTs.[30] They found a TCR of 5.9-8.0×10^{10} K/W. Another study performed an MD simulation of SWCNTs at contact at a 90° junction and found a TCR of around 2×10^{10} K/W.[31] These studies confirmed that the fiber-matrix and fiber-fiber thermal contact resistance greatly hinders heat transfer in CNT composites. The TCR between Si nanowires has also been studied using MD simulations and found a TCR around 10^{-9} m^2K/W.[32]

2.8. Experimental Methods

Different attempts have been made to experimentally measure the thermal contact resistance between crossed micro fibers and wires. Yang *et al*. measured the TCR between individual CNTs.[33] Using a microdevice, they measured the total thermal resistance of the two CNTs together, and then subtracted the thermal resistance of CNTs based on their

thermal properties measured separately; the remainder is the TCR. They reported a thermal contact resistance on the order of 10^8 K/W, which is more than an order of magnitude lower than that predicted from MD simulations.[30,31]

Guo *et al*. investigated heat transfer in arrays of aligned TiO_2 nanotubes.[34] The thermal contact resistance between the TiO_2 nanotubes was measured in the process. The photothermal method was used to measure the effective thermal conductivity in the axial direction. The TET method was then used to measure the properties in the cross-tube direction. The thermal contact resistance was calculated from the measured effective properties and the geometry of the samples. The TCR in this study was the resistance in the cross tube direction between parallel tubes in contact. The TCR was determined to be around 15-20 m^2K/W for amorphous TiO_2 samples and around 5.9 m^2K/W for anatase samples.

Another experimental method to measure the TCR between crossed fibers is a T-type probe technique, which shall be discussed in more detail in the next section.

2.9. T-type Probe Technique

The T-type probe is a method that has been developed to measure the thermal properties of thin wires and fibers.[35] It can also be used to measure the thermal contact resistance between crossed wires/fibers.

The T-type probe method consists of a hot wire whose ends are connected to heat sinks that are held at a constant temperature. One end of the to-be-measured sample is attached to the center of the hot wire and the other end to a heat sink held at constant temperature. The steady state one-dimensional heat transfer equation is solved for each of the

wires, with appropriate boundary conditions. The thermal conductivity is found by fitting the measured temperature change in the hot wire to the analytical solution. Initially the thermal contact resistance between the sample and hot wire was ignored.[35] In later measurements, the TCR was accounted for by taking multiple steady state measurements with different length samples.[36]

The T-type probe method was modified to measure the thermal effusivity, $b = \sqrt{k\rho c_p} = k/\sqrt{\alpha}$, of a thin wire or fiber.[37] In the steady state technique, a dc is fed through the hot wire. In the modified technique, an ac is fed through the hot wire, similar to the 3ω method. The measurement takes place in two stages. First a 3ω measurement is done to calibrate the properties of the hot wire. Then the sample is connected to the hot wire and a 3ω measurement is done again. The effusivity of the sample and the TCR are fitted to a dimensionless heat transfer function derived from the solution the heat equation in the wires.

To ensure good thermal contact between the hot wire and the sample wire, an interfacial material is used to make the contact, resulting in a low TCR. In this case, the measured TCR between Pt wires was from 3600 to 18800 K/W.[37] In this case, the measured TCR is essentially the thermal resistance of the bonding material. If no material is used to enhance the contact, the T-type probe can be used to measure the TCR of bare contact between microwires. Wang *et al.* measured the TCR between Pt wires at a temperatures from 100-300K.[38] They made an attempt to predict the TCR based on the deflection of the wires due to contact and the wires' material properties. In their paper, they reported a dimensionless TCR defined as $R_c^* = R_c k S_c / \sigma$, where S_c is the contact area, and σ is the

standard deviation of the surface roughness of the samples. Using some assumptions about the Pt wire samples, this corresponds to a TCR on the order of 10^5-10^6 K/W.

2.10. Textile Heat Transfer

As mentioned earlier, one possible area where the results of this work can be applied is the heat transfer in fiber composite materials.[40] Another possible application is in the modeling of heat transfer in woven textiles. When measuring heat transfer in textile materials, the textile is often treated as a continuous material and effective thermal properties are measured.[41] Modeling heat transfer in textiles is very complicated and can quickly become intractable, especially if mass transfer through the material is also considered.[42] Finite element methods are often used.[43] Measuring the thermal contact resistance between individual fibers could simplify the problem significantly and be used to make better predictions of heat transfer through woven fiber materials.

Chapter 3. Problem Statement

The main purpose of this research is to develop a technique to measure the thermal contact resistance between two crossed microfibers or wires. In doing so, what is being characterized is essentially zero-dimensional heat transfer; or heat transfer across a single point. This has not been done before in the context of a thermal contact resistance.

The research is done in two parts, as will be described in the following sections. The first part is to demonstrate the effective use of existing one-dimensional techniques to characterize the heat transfer properties of micro/nanoscale materials. Specifically, the photothermal and TET techniques were used to measure the properties of thin films and microfibers/wires, respectively.

Secondly, the main focus of this work is to develop a technique based on a modified TET method to measure the thermal contact resistance between two crossed microwires, which will be called the contact transient electrothermal (CTET) technique. Currently there are few ways to determine the thermal contact resistance in a configuration like this. The only comparable technique is the T-type probe method, described in section 2.9. However, the T-type probe can only give a dimensionless normalized TCR. To obtain an actual value for the TCR, information about the contact area, surface roughness of the samples and sample mechanical properties must be known. The CTET technique is straightforward and directly determines the value of the thermal contact resistance in units of K/W. The CTET technique also has the same advantage over the T-type probe that the TET technique has over the 3ω method. That is, it requires a much shorter measurement time, less than a second, and

has a superior signal to noise ratio. Also, if the thermal properties of the sample are known, only one measurement is required.

There are several applications where knowing the thermal contact resistance between crossed fibers may be desired. One application is in nanofiber composite materials. As described in section 2.7., the thermal transport in these composites is limited in part by the contact resistance between fibers. Another important application may be to help simplify the modeling of heat transfer in woven textile materials.

Chapter 4. One-dimensional Micro/Nanoscale Thermal Transport

4.1. Photothermal Method

As mentioned in section 2.3., a one-dimensional multilayer heat transfer model was developed by Hu *et al.*[15] and applied to a photothermal method for measuring the thermophysical properties of thin films.[16] A cross sectional view of an *N*-layer sample is shown in Figure 1. For an incident laser beam with energy flux $I = I_0\left(1+\cos\omega t\right)/2$, the governing equation for the i^{th} layer is

$$\frac{\partial^2\theta_i}{\partial x^2} = \frac{1}{\alpha_i}\frac{\partial\theta_i}{\partial t} - \frac{\beta_i I_0}{2k_i}\exp\left(\sum_{m=i+1}^{N} -\beta_m L_m\right)e^{\beta_i(x-l_i)}\left(1+e^{j\omega t}\right). \tag{3}$$

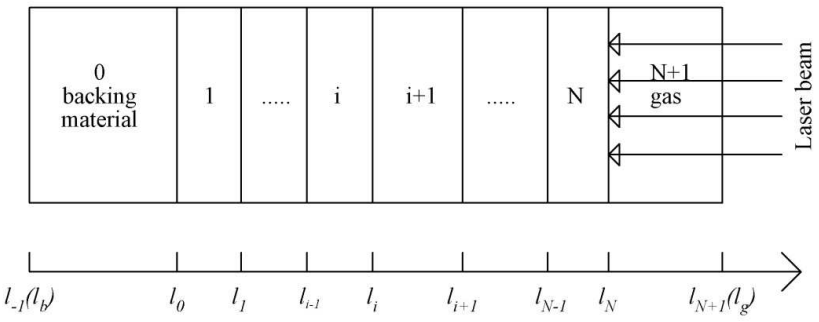

Figure 1: Cross sectional view of multilayer sample for photothermal measurement

Here $\theta_i = T_i - T_{amb}$ for ambient temperature T_{amb}, α_i, k_i and β_i are the thermal diffusivity, thermal conductivity, and optical absorption of layer *i*, respectively, and $j = \sqrt{-1}$. The third term in this equation is the heat source term that comes from the absorption of the laser. Only the steady alternating component of the solution, $\tilde{\theta}_{i,s}$, is considered. This component of the solution to equation (3) is

$$\tilde{\theta}_{i,s} = \left[A_i e^{\sigma_i (x-h_i)} + B_i e^{-\sigma_i (x-h_i)} - E_i e^{\beta_i (x-h_i)} \right] e^{j\omega t} \tag{4}$$

where A_i, B_i are coefficients that can be determined from

$$\begin{bmatrix} A_i \\ B_i \end{bmatrix} = U_i \begin{bmatrix} A_{i+1} \\ B_{i+1} \end{bmatrix} + V_i \begin{bmatrix} E_i \\ E_{i+1} \end{bmatrix}. \tag{5}$$

The physical meaning of U_i is the transmission matrix of heat between layers, including the effect of thermal contact resistance. The physical interpretation of V_i is the absorption matrix of the laser. A more complete derivation and explanation of the coefficients is given in Appendix A based on reference (15).

From the above solution, the phase shift between the thermal radiation from the sample's surface and the incident laser can be calculated. This phase shift can be measured and fitted to determine the properties of interest. The principle of this photothermal technique is shown in Figure 2. This photothermal method was used to measure the thermal and physical properties of several different thin film samples. Figure 3 shows the experimental setup used in the photothermal measurements.

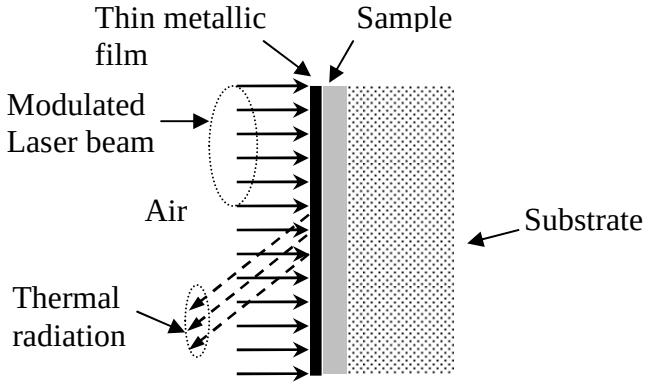

Figure 2: Principle of the photothermal measurement

In the experiment a modulated laser beam is directed onto the sample. The modulated laser has a wavelength of 810 nm. The thermal radiation from the sample is collected by two parabolic mirrors and focused onto an infrared detector. A Ge window is used to filter out the reflected laser beam and only allow through the thermal radiation from the sample. The modulation frequency of the laser is controlled with a function generator (Stanford Research Systems, model DS345), and a lock-in amplifier (Stanford Research Systems, model SR830) is used to obtain the phase shift of the thermal radiation signal at the laser's frequency. Automatic data acquisition is enabled by a personal computer.

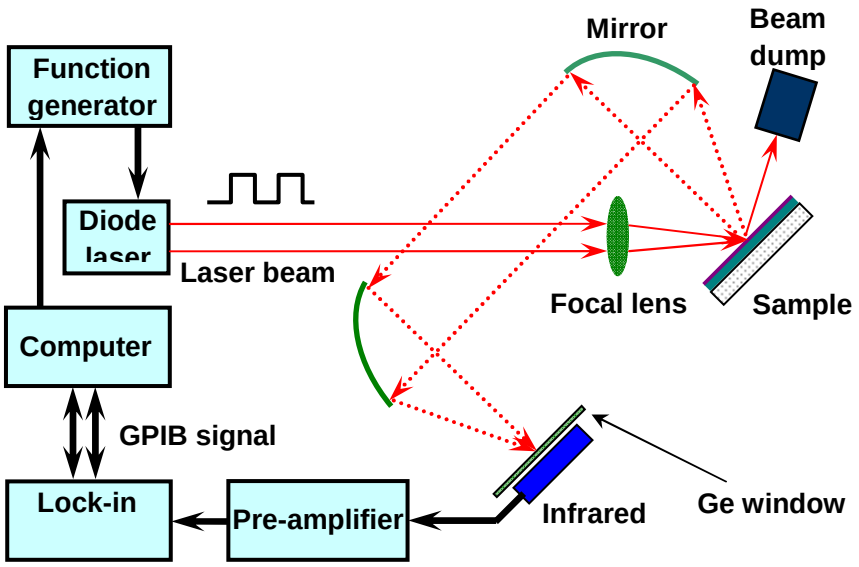

Figure 3: Experimental setup for the photothermal technique

To obtain information about the thermal and physical properties of the sample, the phase shift of the thermal radiation is measured. However, there is an unavoidable time delay induced by the measurement system that could induce significant error into the measurement. To avoid this error, a calibration is done. This is done by measuring the phase shift of the

reflected laser beam on a sample. When a photothermal measurement is performed, this calibration phase shift is subtracted from the measured phase shift before data processing. Figure 4 shows the calibration signal from a Si sample.

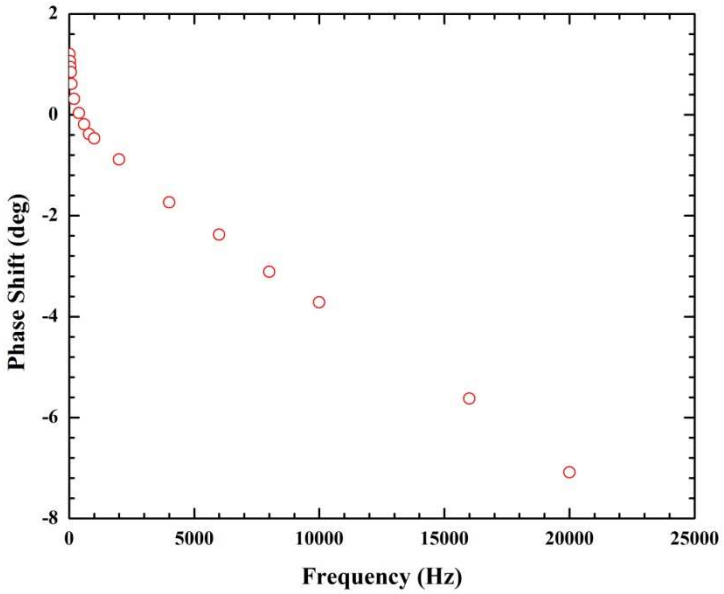

Figure 4: Calibration results for photothermal technique

In performing the photothermal measurement, it is usually beneficial to coat the sample with a thin metallic film layer. This serves as an opaque layer that absorbs all of the laser energy, which is helpful when the light absorption properties of the sample are not known.

The following sections give several examples of photothermal measurements done on a variety of samples.

4.1.1. SiC Film

One sample that was measured using this technique was a SiC thin film deposited on a Si substrate. The SiC film was 2.5 μm thick and had been coated with an 80 nm thick Cr

film. Values of the thermal conductivity k and the thermal contact resistance R_c between sample and substrate were tried to find the best fit between the calculated phase shift and experimental data. The values obtained were k = 3.992 W/mK and $R_c = 1.93\times10^{-7}$ m^2K/W. The non-experimental properties used in the calculations are given in Appendix C and the data fitting for this measurement is shown in Figure 5.

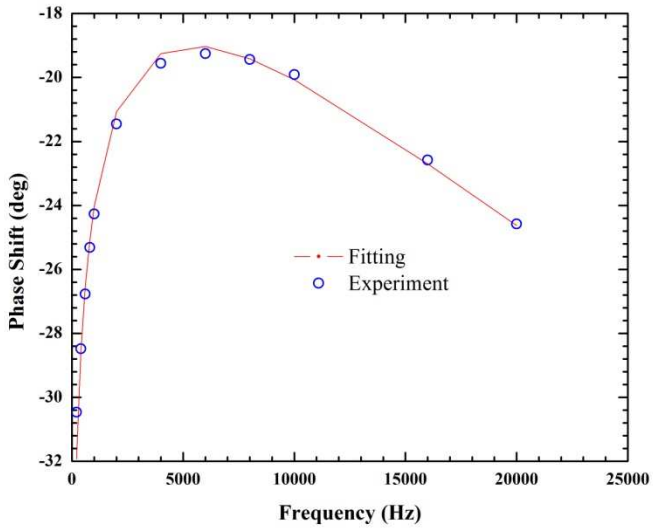

Figure 5: Data fitting for photothermal measurement on 2.5 µm SiC sample

4.1.2. PBL-Al Film

Another sample that was characterized using this method was a 6 µm thick PBL-Al thin film sample deposited on a Si substrate provided by Panasonic. A 100 nm gold layer was sputter coated onto this sample for measurement. In this measurement, values of the thermal conductivity and density were fitted to the experimental data. In order to obtain an accurate value of the density from this measurement, the specific heat must be known. The specific heat was not known for this sample, so the value reported from the measurement was the specific heat capacity, which is the product of the density and specific heat, using an assumed value for c_p. If the correct value of the specific heat is known, the correct value of the density

can easily be found from the specific heat capacity. Three measurements were done on this sample and an average thermal conductivity of 1.46 W/mK and average specific heat capacity of 3.50 J/m^{3}K were found. These values varied less than 5% between measurements. The properties used in the data fitting are given in Appendix D and the measurement results in Table 1. The data fitting for the measurements are shown in Figure 6.

Table 1: Results for PBL-Al photothermal measurement

Measurement	Thermal Conductivity (W/m·K)	Specific Heat Capacity $\rho \cdot c_p$ (J/m^3·K)	Density (kg/m^3)
1	1.493	3.51×10^6	3987
2	1.43	3.39×10^6	3851
3	1.466	3.60×10^6	4086
Average	1.463	3.50×10^6	3975

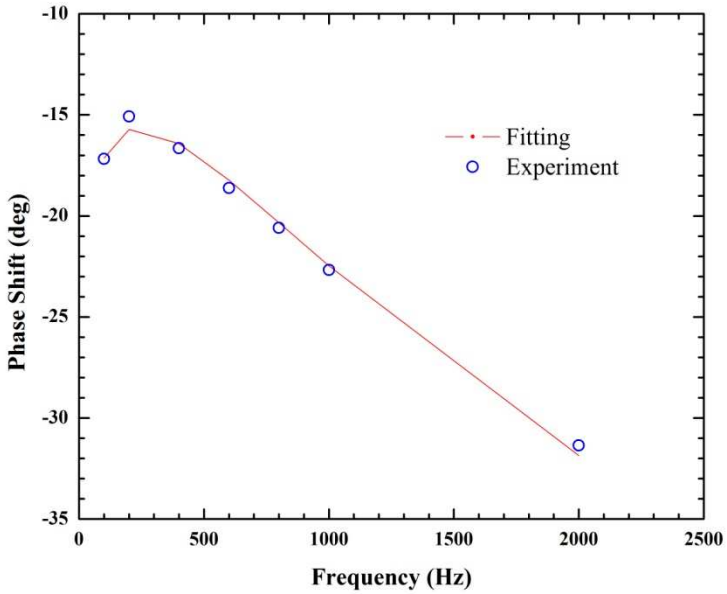

Figure 6: Data fitting for second photothermal measurement of PBL-Al sample

4.1.3. Carbon Films

The following two samples are examples from an ongoing project in collaboration with the Department of Energy's Kansas City Plant and Dr. Pal Molian. The goal of this project is to develop a method of creating diamond-like carbon (DLC) films that have high thermal conductivity. The intent is to use these high thermal conductivity DLC films in the thermal management of high powered electronics. The samples examined here were labeled P3 and P7. These samples are representative of early efforts and consist of primarily amorphous carbon, and have a low thermal conductivity. These samples are deposited on a ceramic substrate known as LTCC. Before measurement, each sample was partially coated with a 200nm layer of Au.

Sample P3 had a thickness of 4μm and was measured to have a thermal conductivity of 3.664 W/m^2K and a density of 1991 kg/m^3. Sample P7 had a thickness of 7μm and was measured to have a thermal conductivity of 6.793 W/m^2K and a density of 927.7 kg/m^3. The non-experimental properties used in the measurement are given in Appendix E. The data fitting for these samples is given in Figures 7 and 8.

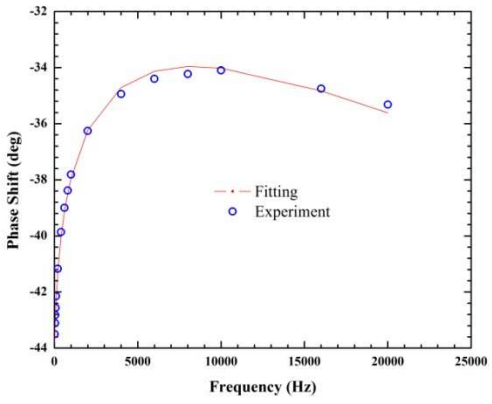

Figure 7: Data fitting for sample P3

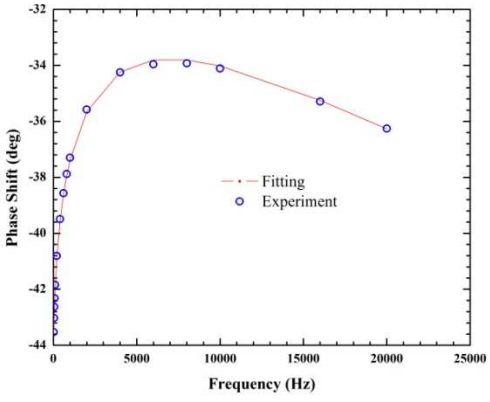

Figure 8: Data fitting for sample P7

4.2. TET Technique

The principle of the TET technique is shown in Figure 9. Assuming that the diameter of the wire is much less than its length, the heat transfer can be considered one dimension in the axial direction. The governing equation for heat transfer in the wire is then

$$\frac{\rho c_p \partial T}{\partial t} = k \frac{\partial^2 T}{\partial x^2} + q_0 \tag{6}$$

for thermal conductivity k, density ρ, and specific heat c_p. q_0 is the electrical heating power from the supplied current and is assumed to be constant. The initial temperature of the wire is $T(x, t = 0) = T_0$, for room temperature T_0. The copper electrodes are much larger than the diameter of the wire, so it is assumed that the boundary conditions at each end of the wire are $T(x = 0, t) = T(x = L, t) = T_0$.

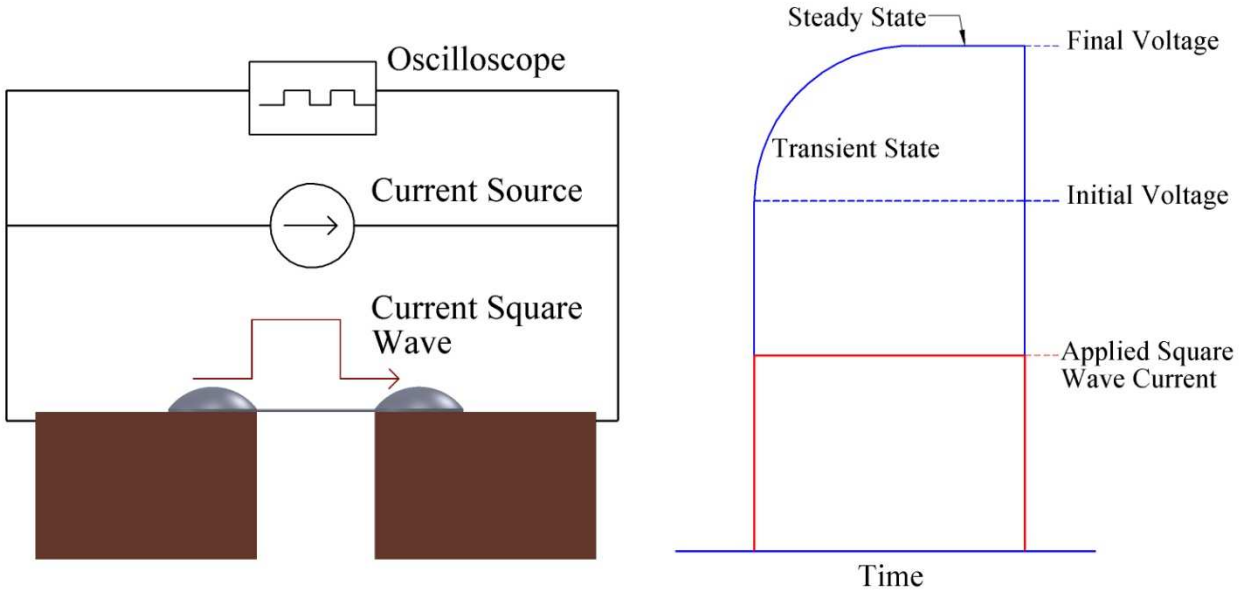

Figure 9: Experimental Principle of the TET technique

A Green's Function integral method is used to find the solution to this PDE. Another integration is performed to obtain the average temperature of the wire. The temperature increase is then normalized as $T^* = [T(t) - T_0]/[T(t \to \infty) - T_0]$, which is found to be

$$T^* = \frac{96}{\pi^4} \sum_{m=1}^{\infty} \frac{1 - \exp\left[-(2m-1)^2 \pi^2 \alpha t / L^2\right]}{(2m-1)^4}. \tag{7}$$

A more complete derivation of this expression can be found in reference (17) and Appendix B. It can be seen from this solution that for any one dimensional sample of any material and of any length, the normalized temperature evolution is exactly the same with respect to a normalized time represented by the dimensionless Fourier number $Fo = \alpha t / L^2$. The recorded voltage increase is related to the temperature increase in the following way:[18]

$$U(t) = IR_0 + I\eta \frac{8q_0 L^2}{k\pi^4} \sum_{m=1}^{\infty} \frac{1 - \exp\left[-(2m-1)^2 \pi^2 \alpha t / L^2\right]}{(2m-1)^4}, \tag{8}$$

where $U(t)$ is the measured voltage, R_0 is the initial resistance of the sample, and η is the temperature coefficient of resistance of the sample. If η is not known, it can be obtained by performing a calibration experiment. In this calibration, the resistance of the sample is measured at several temperatures. The slope of the plotted resistance vs. temperature graph is the η of the sample.

This TET technique has been used extensively in this work. It will be described in Chapter 5 how the TET technique has been modified to characterize the thermal contact resistance between two crossed wires. In this section two examples will be given to illustrate the TET technique.

4.2.1. Pt wire

The TET technique was used to measure the thermal diffusivity of a Pt wire sample. The values obtained by experiment can be compared to reference values for Pt to determine the accuracy of the technique. A 4.5mm Pt wire sample was prepared and a TET experiment was performed. A heating current of 50mA was used. The measured thermal diffusivity was 2.375×10^{-5} m^2/s. This is a 5.4% difference from the reference value of 2.51×10^{-5} m^2/s.[26] The data fitting for this measurement is shown in Figure 10.

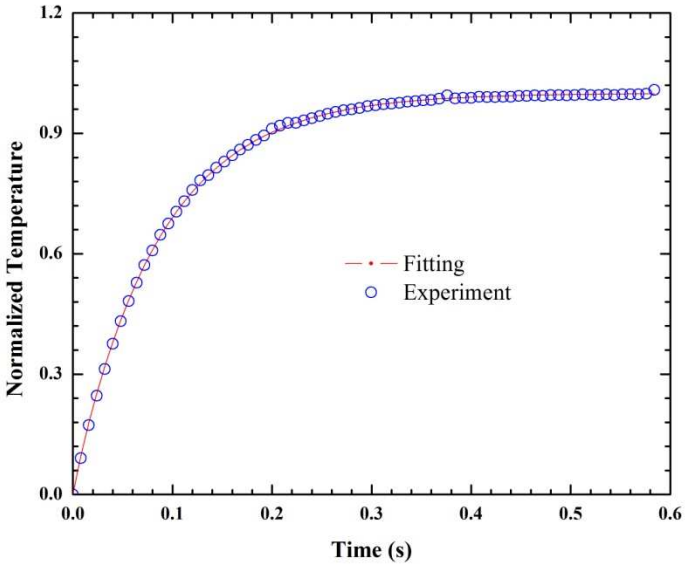

Figure 10: Data fitting for Pt wire TET measurement

4.2.3. Human Hair

The TET technique can be used to measure both conductive and nonconductive micro/nanowires. If the sample is not electrically conductive, it is sputter coated with a very thin layer of Au. The Au coating allows for electrical heating. The Au coating is done before the silver paste is applied to the contact to minimize contact thermal and electrical resistances. The measured α is an effective value that includes the effects of the Au coating. The effect of the Au coating can be accounted for by using the concept of thermal conductance.[17] The thermal

conductance is defined as $G_f = A_f k_f / L$, where A_f and k_f are the cross sectional area and thermal conductivity of the Au film. Since the cross sectional area of the film is difficult to ascertain, and k_f will be smaller than bulk values, the thermal conductance is determined using the Wiedmann-Franz law: $L_{Lorenz} = k/(\sigma T)$ for thermal conductivity k and electrical conductivity σ. The Lorenz number used in this work is 2.45 WΩ/K^2.[1] Assuming that the cross sectional area of the film is much smaller than that of the sample the real thermal diffusivity can be found from

$$\alpha = \alpha_e - \frac{L_{Lorenz} T L}{R A \rho c_p} \tag{9}$$

for room temperature T, initial resistance R, and cross sectional area A. If the density and specific heat of the sample are not known, then the effective thermal conductivity of the sample is found first from

$$k_e = \frac{I^2 R L}{12 A \Delta T}. \tag{10}$$

ρc_p can then be found from the effective thermal diffusivity and effective thermal conductivity. The real value of the thermal conductivity can be calculated as

$$k = k_e - \frac{L_{Lorenz} T L}{R A}. \tag{11}$$

The TET technique was used to measure the thermal diffusivity and thermal conductivity of a human hair sample. The sample was taken from the middle portion of a long hair sample. The sample had a length of 1.98 mm and a diameter of 67 μm. A calibration was done to determine the sample's coefficient of resistance. The results of the calibration are shown in Figure 11. A measurement of the sample with a heating current of 1.5 mA yielded a value for the thermal

diffusivity of 3.025×10^{-7} m^2/s and a thermal conductivity of 2.773 W/mK. The data fitting for this measurement is given in Figure 12.

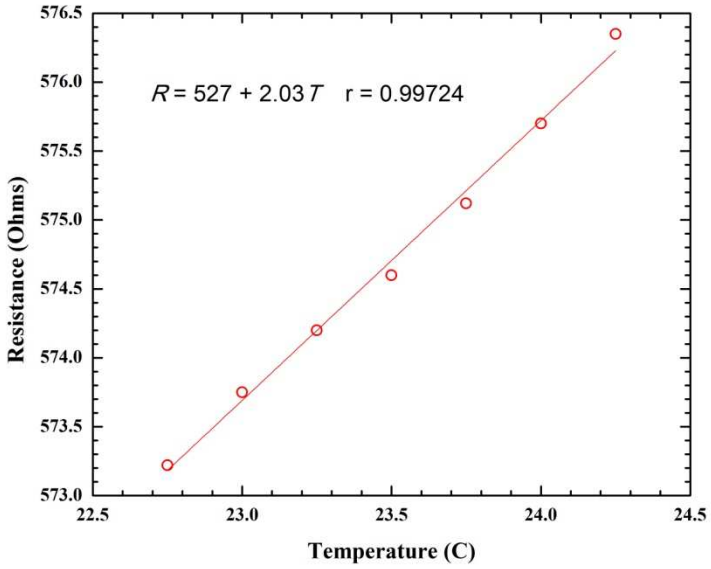

Figure 11: Calibration to determine temperature coefficient of resistance for human hair sample

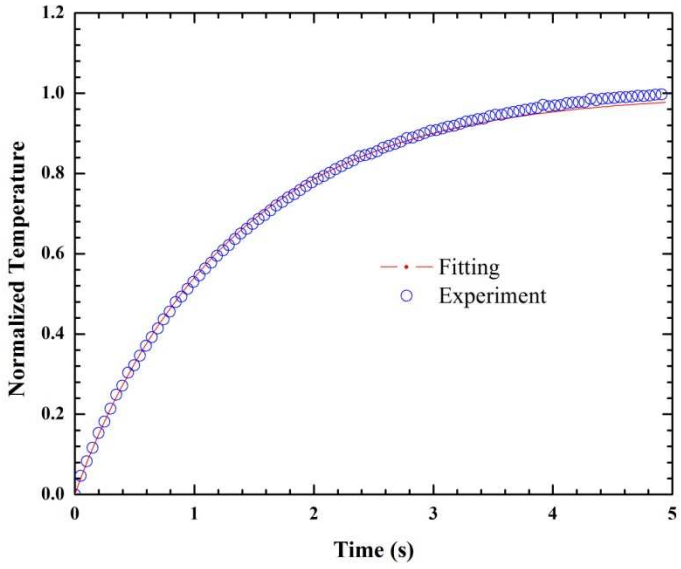

Figure 12: Data fitting for human hair sample TET measurement

Chapter 5. Theory of the CTET Technique

In the transient electrothermal (TET) technique, the sample whose properties are to be measured is suspended between two electrodes. A direct current is then fed through the wire. This current will induce joule heating, causing a temperature change, and in turn a resistance change. This resistance change can be measured by measuring the change in the voltage across the wire. In this way, the temperature evolution can be measured by measuring the voltage evolution. The thermal diffusivity can then be obtained by fitting the measured temperature change to a theoretical curve. This method is described in more detail in section 4.2. and reference (17).

The concept is similar for the contact transient electrothermal (CTET) technique. However, in this experiment, the quantity to be measured is not the thermal diffusivity of the sample, but the thermal contact resistance between two crossed fibers or wires. In this technique a top sample is mounted in a manner similar to a sample in the TET measurement. That is, the sample is suspended between two copper electrodes, with the electrical contact made by applying colloidal silver paint. In addition, a bottom sample is mounted in a similar manner onto a second stage, suspended between two electrodes. A schematic of the experimental principle is shown in Figure 13. A step direct current is fed through the top sample to induce joule heating, as in the TET technique. However, when there is another fiber or wire in contact with the top sample, some heat will be conducted into the bottom sample, lowering the average temperature of the top sample. This temperature evolution will be qualitatively different than that obtained from a single fiber TET measurement given the same heating current in two ways. First, the final steady state temperature will be lower than in a single fiber. Second, the fiber in contact will reach steady state quicker than a single fiber.

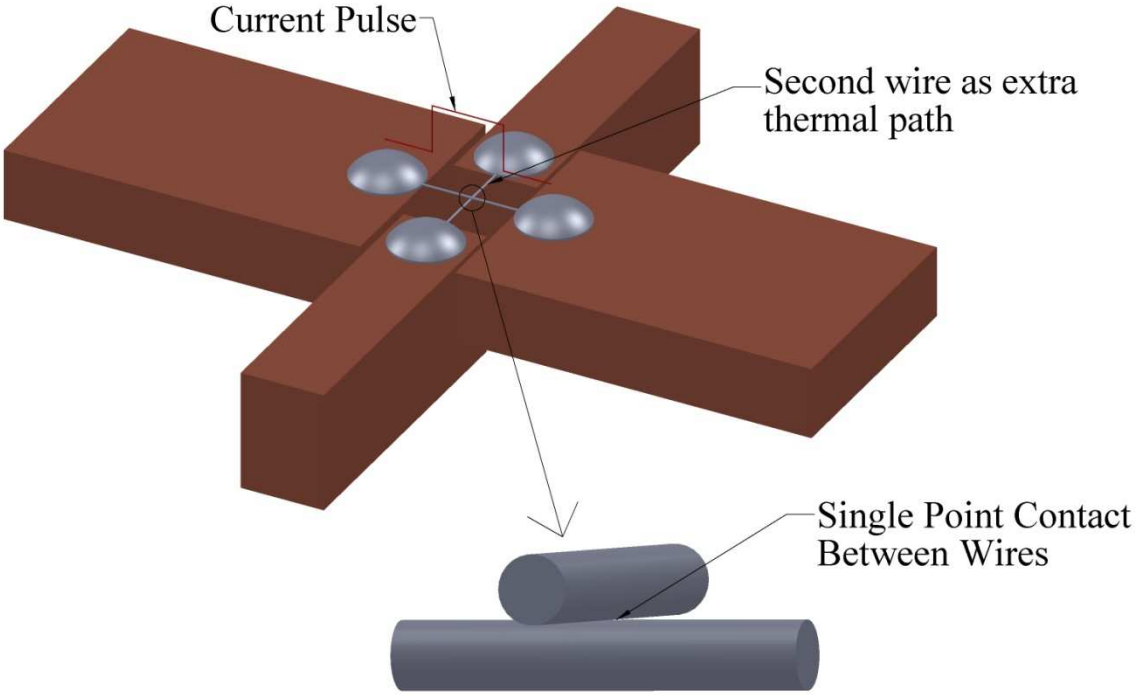

Figure 13: Experimental Principle of CTET measurement

The thermal properties of the samples such as thermal conductivity, density, and specific heat, must be known in order to measure the thermal contact resistance with this technique. These properties can be either found from the literature, or can be determined from a separate TET measurement of the single wire.

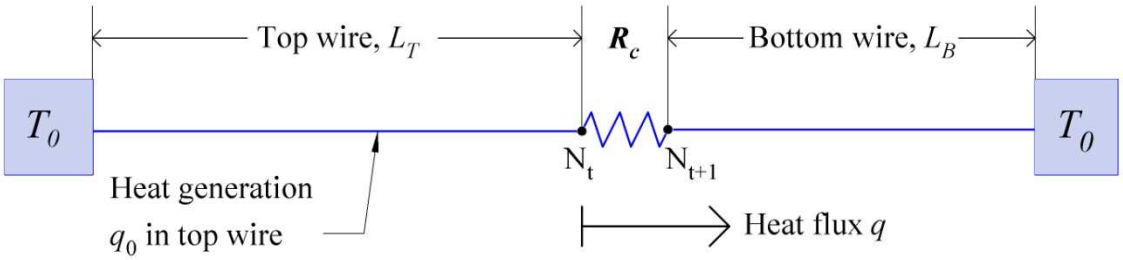

Figure 14: Heat transfer model for CTET technique using symmetry assumption

To calculate the thermal contact resistance between the two fibers, the problem is assumed to be symmetrical about the contact point, so that half the length of both the top and bottom fiber can be considered in the heat transfer analysis as shown in Figure 14. This condition can be met by carefully positioning the bottom wire to make sure it is in contact with top wire at their midpoints. Two methods have been developed to calculate the value of the thermal contact resistance from the measured voltage/temperature evolution. The first one is a steady state analytical solution where the contact resistance is determined from the final average temperature of the top sample. The second one is based on a transient numerical solution by fitting the transient response of the top wire under step electrical heating. In this method, the temperature distribution in the samples is calculated numerically and used to determine an average temperature evolution. Trial values for the thermal contact resistance are used to calculate the temperature evolution until a value is found that gives the best fit (least square fitting) with the experimental data. These two methods are described in the next sections.

5.1. Analytical Solution

When the fibers in contact have reached steady state, it may be expected that they would have a temperature distribution similar to that in Figure 15.

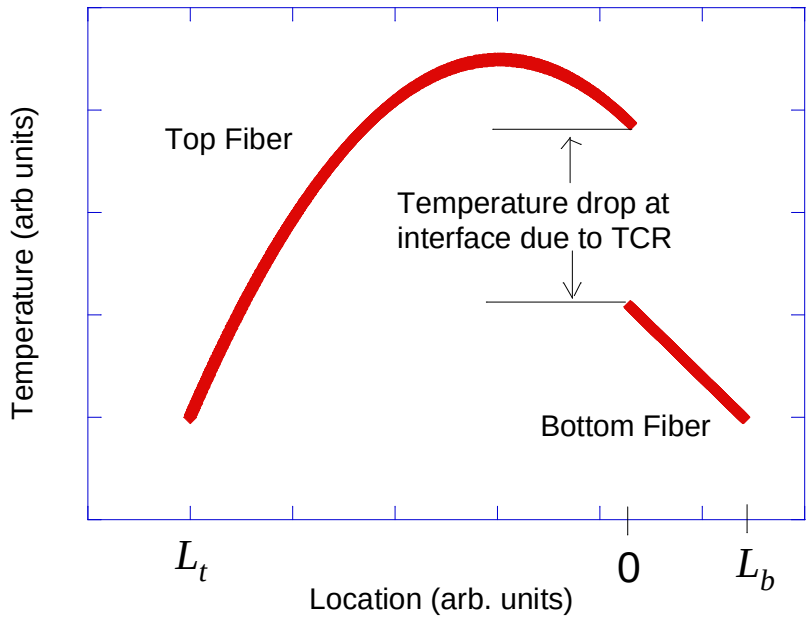

Figure 15: Steady state temperature distribution in CTET samples

The temperature profile in the bottom fiber will be a linear function of position, while the temperature profile in the top fiber has a more complicated shape due to the joule heating and heat conduction within the fiber. Taking the contact point as the origin, there is a temperature jump between the top and bottom fibers at $x = 0$ due to the thermal contact resistance, and we would expect the temperature of the top fiber at the contact to be higher than that of the bottom fiber. We shall designate the temperature of the top fiber at $x = 0$ as $T(0)$, and the temperature of the bottom fiber at $x = 0$ as T_B. For the bottom fiber, the governing equation for one dimensional heat transfer with no heat generation is[39]

$$k_B \frac{dT}{dx} = q \tag{12}$$

for thermal conductivity of the bottom fiber k_B and constant heat flux q. We set the boundary conditions for the bottom fiber to be $T(L_B) = 0$ and $T(0) = T_B$. Solving this equation we get

$$T_B = \frac{qL_B}{k_B}. \tag{13}$$

By the definition of thermal contact resistance R_c, we get the relationship between the top and bottom fiber temperatures at $x = 0$:

$$q = \frac{T(0) - T_B}{R_c}. \tag{14}$$

Equations (13) and (14) can be combined to get

$$T(0) = q\left(R_c + \frac{L_B}{k_B}\right). \tag{15}$$

The governing equation for the top fiber considering one dimensional heat transfer with constant heat generation $\dot{q}$ is[39]

$$\frac{d^2T}{dx^2} + \frac{\dot{q}}{k_T} = 0 \tag{16}$$

where k_T is the thermal conductivity of the top fiber. This is subject to the boundary conditions $T(L_T) = 0$ and $\left.\frac{dT}{dx}\right|_{x=0} = \frac{q}{k_T}$. The solution to this equation is

$$T(x) = -\frac{\dot{q}}{2k_T}x^2 + C_1 x + C_2. \tag{17}$$

From the first boundary condition we get $C_1 = \frac{q}{k_T}$ and from the second boundary condition we find $C_2 = \frac{\dot{q}L_T^2}{2k_T} - \frac{qL_T}{k_T}$. Substituting C_1 and C_2 into equation (17) gives

$$T(x) = \frac{\dot{q}}{2k_T}\left(L_T^2 - x^2\right) - \frac{q}{k_T}\left(L_T - x\right). \tag{18}$$

An expression for the heat flux q is found by combining equations (15) and (18):

$$T(0) = q\left(R_c + \frac{L_B}{k_B}\right) = \frac{\dot{q}L_T^2}{2k_T} - \frac{qL_T}{k_T}. \tag{19}$$

Rearranging, and defining a total thermal resistance R as $R = R_c + \frac{L_B}{k_B} + \frac{L_T}{k_T}$, shows the heat flux to be

$$q = \frac{\dot{q}L_T^2}{2k_T R}. \tag{20}$$

The steady state temperature distribution in the top fiber is then

$$T(x) = \frac{\dot{q}}{2k_T}\left(L_T^2 - x^2\right) - \frac{\dot{q}L_T^2}{2k_T^2 R}\left(L_T - x\right). \tag{21}$$

The steady state average temperature of the top wire can then be found as

$$\bar{T} = \frac{1}{L_T}\int_0^{L_T} T(x)dx = \frac{\dot{q}L_T^2}{2k_T}\left(\frac{2}{3} - \frac{L_T}{2k_T R}\right). \tag{22}$$

Rearranging and substituting back in the definition of the total thermal resistance R, the thermal contact resistance between the two crossed wires can be written as

$$R_c = \frac{3\dot{q}L_T^2 / 4k_T}{\dot{q}L_T - 3\bar{T}k_T / L_T} - \left(\frac{L_T}{k_T} + \frac{L_B}{k_B}\right). \tag{23}$$

The value obtained from this equation is in reality twice the actual thermal contact resistance. Since the heat transfer model uses a symmetry assumption, only half of the heat transported through the contact point is considered. The reported values of the TCR in later sections are the values obtained from this equation divided by two. This expression also calculates the thermal contact resistance in units of m^2K/W. It is more convenient for later comparison with the numerical calculation to give the thermal contact resistance in units of K/W. For this reason, the value from equation (23) is then divided by the cross sectional area of the top fiber, A_T. In this analysis the temperature is normalized so that the initial temperature is zero. Therefore, in the above expression, the final average temperature of the top wire $\bar{T}$ is simply the final temperature increase measured in the experiment. It should also be noted that the lengths L_T and L_B in the above expression are actually half the measured length of the fibers due to the symmetry assumption used in the derivation. The volumetric heat generation is due to Joule heating in the top wire:

$$\dot{q} = \frac{I^2 R_f}{L_T A_T}. \tag{24}$$

Here I is the heating current in Amperes, R_f is the final resistance of the sample in Ohms, L_T is the full length of the top fiber and A_T is the cross-sectional area of the top fiber. Heat transfer from convection and radiation is assumed to be negligible in this analysis.

5.2. Numerical Solution

The governing equation for the time-dependent heat transfer in the top and bottom fibers in the CTET experiment is that for one-dimensional heat transfer with heat generation:[39]

$$\rho c_p \frac{\partial T}{\partial t} = k \frac{\partial^2 T}{\partial x^2} + \dot{q} \tag{25}$$

where k is the thermal conductivity, ρ is the density, and $c_p$the specific heat of the sample. In the top fiber, the volumetric heat generation $\dot{q}$ is the Joule heating. In the bottom fiber, the heat generation is zero. Convection and radiation heat transfer are assumed to be negligible.

To solve this equation numerically, a one-dimensional implicit Euler finite difference scheme is used.[44] This scheme is first order accurate in time, and second order accurate in space, and because it is an implicit scheme, it is unconditionally stable for all combinations of Δx and Δt. The Δt used in the calculation was 20 μs. The Δx used was such that the top wire was divided into 1000 grid points and the bottom wire was divided into 500 grid points. For approximating the temperature at time $t = (n+1)\Delta t$ and position $x = i\Delta x$, the finite difference equation is

$$\rho c_p \frac{T_i^{n+1} - T_i^n}{\Delta t} = k \frac{T_{i-1}^{n+1} - 2T_i^{n+1} + T_{i+1}^{n+1}}{\Delta x^2} + \dot{q}. \tag{26}$$

The volumetric heat generation is $\dot{q} = \frac{q_0}{A\Delta x}$ where A is the cross-sectional area of the sample and q_o is the joule heating in Watts that occurs in the element Δx. It is defined as

$$q_0 = I^2 R \frac{\Delta x}{L_T} \tag{27}$$

where R is the sample resistance and L_T is the full length of the sample. Equation (26) then becomes

$$\rho c_p \frac{T_i^{n+1} - T_i^n}{\Delta t} = k \frac{T_{i-1}^{n+1} - 2T_i^{n+1} + T_{i+1}^{n+1}}{\Delta x^2} + \frac{q_0}{A\Delta x}. \tag{28}$$

This equation can be rearranged to find the following:

$$-\frac{kA}{\Delta x}T_{i-1}^{n+1}+\left(\frac{2kA}{\Delta x}+\frac{\Delta x}{\Delta t}\rho c_p A\right)T_i^{n+1}-\frac{kA}{\Delta x}T_{i+1}^{n+1}=\frac{\Delta x}{\Delta t}\rho c_p A T_i^n+q_0. \tag{29}$$

This becomes a set of linear equations to find the temperatures at every point at time $t=(n+1)\Delta t$ that must be solved simultaneously. When put into matrix form, this set of equations form a tri-diagonal matrix, which lends itself to an easy solution using the Thomas algorithm.[44]

To use this method, we define four coefficients a, b, c and d for each equation so that

$$aT_{i-1}^{n+1}+bT_i^{n+1}+cT_{i+1}^{n+1}=d. \tag{30}$$

The coefficients for interior points can be found from equation (29). For the constant temperature boundary conditions at $x=0$ and $x=\left(\frac{1}{2}L_T+\frac{1}{2}L_B\right)$, where the temperature is defined to be zero, the coefficients $a=0$ and $c=0$, respectively.

To consider the thermal contact resistance in the numerical analysis, it is treated as if there is a fictional discrete element Δx between the two fibers at the contact point. Referring to Figure 14, at the point of contact for the top fiber, point N_T, the coefficient $c=1/R_c$, where R_c has units of K/W. Similarly at point N_t+1, the point of contact for the bottom fiber, the coefficient $a=1/R_c$.

When the coefficients have been defined for all the points in the computational domain, the equations can be solved using the Thomas algorithm.[44] This involves defining two new coefficients p and q as

$$p(i)=\begin{cases}\dfrac{c(i)}{b(i)-a(i)p(i-1)} & i=2,N-1\\ \dfrac{c(i)}{b(i)} & i=1\end{cases}\quad and\quad q(i)=\begin{cases}\dfrac{d(i)-a(i)q(i-1)}{b(i)-a(i)p(i-1)} & i=2,N\\ \dfrac{d(i)}{b(i)} & i=1\end{cases}. \tag{31}$$

The temperatures can then be solved for by working backwards from $i = N$:

$$\begin{aligned}T(N)&=q(N)\\ T(i)&=q(i)-p(i)T(i+1)\end{aligned}. \tag{32}$$

When the temperature distribution over the length of the fibers is known for each time step, an average temperature over the top fiber is found in order to give the average temperature evolution.

In the TET technique, the measured temperature evolution is normalized and fitted to a theoretical curve. For a single wire or fiber that is not in contact, the normalized curve is independent of the actual temperature of the sample. However, for the CTET technique, it is the actual temperature rise that is fitted to a theoretical curve. In order to do this fitting, the actual temperature rise in the sample must be known. First, the change in electrical resistance of the sample is found from the change in voltage across the sample assuming simple Ohm's law behavior. Then the temperature change is calculated from knowledge of how the resistance changes with temperature. The relationship between temperature change and change in electrical resistance depends on the material of the sample and will be described later in section 6 for each material examined.

With the measured temperature increase known, and a numerical scheme developed to calculate a theoretical temperature increase for a given thermal contact resistance, different values of R_c can be tried until the numerically calculated temperature evolution best fits the experimental data. A least squares fitting algorithm is used to find the best fit value of the

thermal contact resistance. Again, because a symmetry assumption is used and only half the heat transferred through the contact point is considered, the actual value of the thermal contact resistance is half of the value obtained by the data fitting program and is reported as such.

Chapter 6. Experiment for Single Point Thermal Resistance Characterization

Figure 16 shows a diagram of the experimental setup. It is similar in design and operation to the experimental setup in the TET technique, but with an additional base holding the bottom sample in contact with the top sample. During the CTET experiment, a step direct current is passed through the top sample to generate Joule heating. The current is supplied by a low noise Keithley 6221 current source. The low noise current source is crucial to providing a sharply rising step current to reduce uncertainty in the measured temperature evolution. This heating will increase the temperature of the top sample and cause a resistance change. The temperature change in the top sample is dependent on not only the properties of the sample, but also the thermal contact resistance between the samples. This resistance change can be measured by measuring the voltage change across the top wire. This voltage change is measured and recorded with a high speed digital oscilloscope model Tektronix TDS 7054.

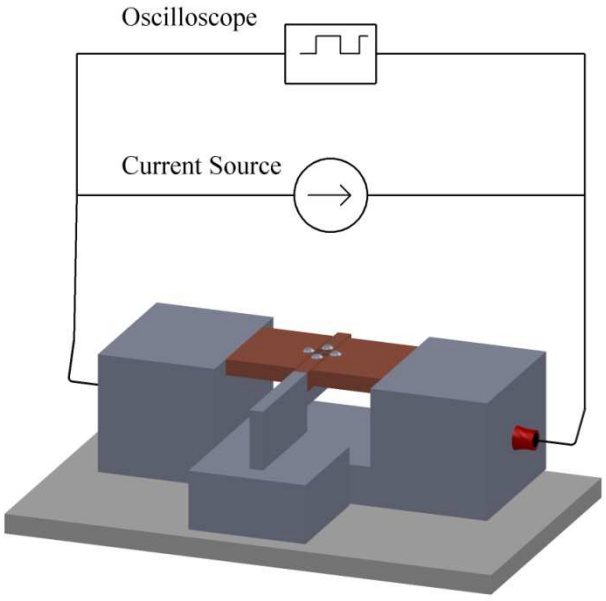

Figure 16: Experimental Setup for the CTET technique

The top sample is mounted between two copper electrodes and secured with colloidal silver paste. The silver paste provides both a good electrical contact and a good thermal contact so that the constant temperature boundary condition can be used in the data analysis. The base on which the top sample is suspended is designed to allow room for the bottom sample. The bottom sample is also suspended between two copper electrodes and secured with silver paste. The bottom base is specially designed to allow for good contact between the fibers, but not interfere with the flow of current through the top fiber. In the experimental setup, the top base is fixed and the bottom base is attached to a three-dimensional microstage. Using the dials on the microstage, the bottom sample can be positioned precisely so that the contact point is approximately in the middle of both samples. The bottom sample is then raised slowly to ensure there is solid contact, but not raised far enough that the samples are bent.

The experiment takes place in a vacuum chamber evacuated to a pressure below 1×10^{-3} Torr to minimize the influence of air convection. At this pressure and room temperature, the mean free path of air molecules is on the order of several centimeters, while the diameters of the samples are on the order of tens of microns.[1,4] This has the effect of making heat transfer to the air negligible.

6.1. Pt Wire Contact Measurement

This technique to measure the thermal contact resistance between two crossed wires was first tested with crossed platinum wires. Platinum wires of diameter 25.4 μm supplied by Omega Engineering were mounted on the top and bottom stage. The bottom wire was made shorter than the top wire to ensure that the thermal resistance of the bottom wire was small compared to the thermal contact resistance. Two sets of samples were prepared and tested with a range of heating currents. Bulk properties of platinum were used in the data processing calculations, with the

exception of the value for the specific heat used in the numerical calculations. In order to obtain a good data fitting, a value for the specific heat that is approximately 9% higher than the bulk value is used. This is considered reasonable due to the uncertainty in the measurements. One possible explanation of this necessity is the influence of the heat capacitance of the electrodes near where the sample is mounted. The properties used in the calculation are listed in Table 2.

In order to perform the numerical calculations, knowledge of how the sample electrical resistance changes with temperature is needed. For metals, the electrical resistance of a wire is given by $R = \rho(T)(L/A)$, where ρ is the electrical resistivity as a function of temperature and L and A are the length and cross-sectional area of the wire, respectively. For platinum wire, the resistivity varies as[45]

$$\rho(T) = \rho_0\left(1+\eta\left(T-T_0\right)\right). \tag{33}$$

Here η is the temperature coefficient of resistance and ρ_0 is the electrical resistivity at a reference temperature T_0. Values of η and ρ_0 for a reference temperature of 20°C are given in Table 2. This equation was used along with the measured length and known diameter of the samples to calculate the initial resistance, rather than measuring the initial resistance. Because Pt wire is highly conductive, the resistance of the samples is on the same order as the total resistance of the electrodes and measurement leads, thus relying on measured resistances can introduce significant error into the measurement.

Table 2: Properties used in Pt wire CTET measurement

Thermal Conductivity	71.6 W/mK
Specific Heat	145 J/kgK
Density	21450 kg/m^3
Temperature Coefficient of Resistance	0.003927 K^{-1}
Resistivity at 20°C	0.106 x 10^{-6} Ωm
Diameter	25.4 μm

6.2. Pt wire Results

The measured values of the thermal contact resistance between two crossed Pt wires vary by approximately one order of magnitude. The values range from about 1.8×10^5 K/W to 1.4×10^6 K/W. The measured thermal contact resistance increases with increased heating current. The steady state analytical model and the transient numerical model seem to generally agree with each other. Two sets of samples were prepared and tested with heating currents ranging from 20mA to 50mA. The experimental conditions and results are listed in Table 3. Taking as an example the first sample set measured at 50mA, the steady state analytical solution gives a resistance of 8.234×10^5 K/W and the numerical solution gives a resistance of 8.427×10^5 K/W. This is in agreement within 3%. The fitting of the experimental data to the numerically calculated temperature rise in the top wire for this sample set is shown in Figure 17. The data fittings for the additional measurements are given in Appendix F. The analytical and numerical values of the thermal contact resistance for each measurement are plotted in Figure 18.

Table 3: Experimental conditions and results for Pt wire CTET

Sample Pair	Top wire length (mm)	Bottom fiber length (mm)	Heating Current (mA)	Resistance of Sample (Ohms)	Steady State Temp. Rise (K)	Analytical Rc (K/W)	Numerical Rc (K/W)
1	4.25	0.96	50	0.896	22.9	5.420×10^5	5.571×10^5
1	4.25	0.96	50	0.896	22.6	4.117×10^5	4.214×10^5
2	4.22	1.00	20	0.890	2.9	8.985×10^4	8.943×10^4
2	4.22	1.00	30	0.890	6.9	1.296×10^5	1.035×10^5
2	4.22	1.00	40	0.890	14.1	7.050×10^5	4.420×10^5

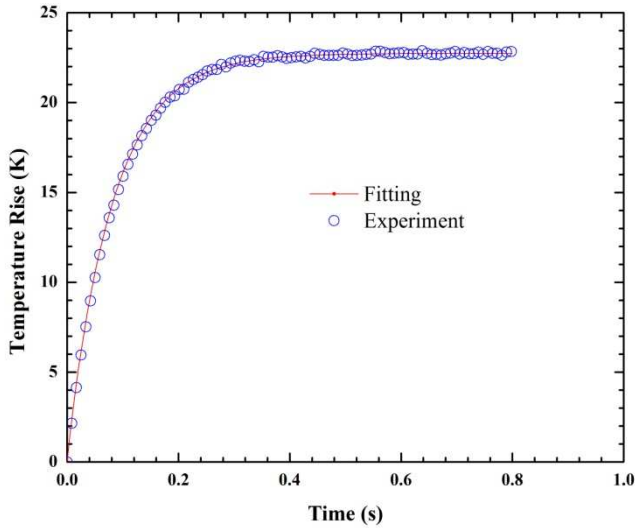

Figure 17: Data fitting for Pt wire CTET measurement

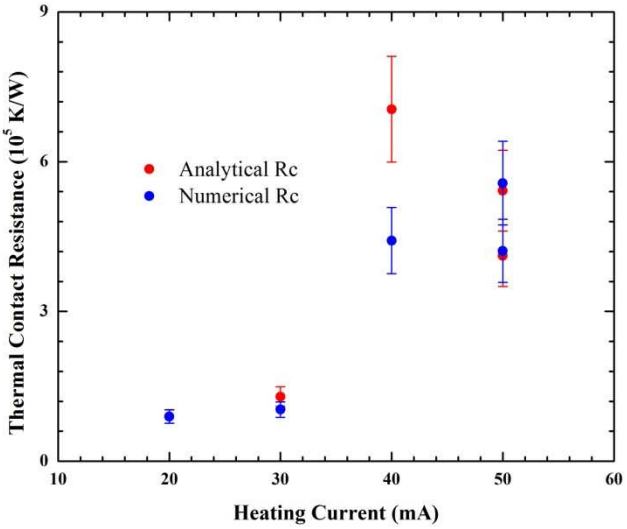

Figure 18: Thermal contact resistance at different heating currents. Bars indicate 15% uncertainty.

6.3. Glass Fiber/Pt Wire Measurement

This method was also used to measure the thermal contact resistance between a glass fiber and a platinum wire. As in the TET technique, the CTET technique can also be used for measuring nonconductive wires/fibers. To do this, the fiber is coated with a thin Au film to enable electrical heating. To ensure good thermal and electrical contact at the electrode, the glass fiber is coated first and then the silver paste is applied. The sample is coated for 50 s in a Denton Vacuum Desk V sputter coater, which deposits an Au coating which is in the range of tens of nanometers thick. The coating is also primarily on the top side of the fiber, leaving the bottom half of the fiber bare. Therefore, the thermal contact resistance measured in the experiment is not influenced by the Au coating.

The glass fibers were provided by Mo Sci Specialty Products and have a known diameter of 9.17 μm. Unlike the Pt wire, the properties of the glass sample are not known. They must be measured separately before the CTET measurement can be done. The density ρ was measured by a member of our lab to be 2070 kg/m^3. The value of the specific heat, c_p, was found from the literature.[46] A TET measurement is done on the glass fiber sample alone, and an effective thermal diffusivity α_e is obtained. This is an effective value because it includes the influence from the Au coating, but this is fine for the purpose of the CTET measurement. An effective thermal conductivity for the sample is calculated from the definition of the thermal diffusivity as

$$k_e = \alpha_e \left(\rho c_p \right). \tag{34}$$

Here the Au coating is assumed to be thin enough compared to the diameter of the fiber that it will not have an effect on the effective ρc_p. The average temperature rise for the fiber during the experiment is found from equation (10):

$$\Delta T = \frac{I^2 R_f L}{12 k_e A}. \tag{35}$$

This temperature rise can be used with the measured final change in resistance to calculate how the resistance changes with temperature, assuming a linear relationship: $dR/dT = \Delta R/\Delta T$. It is assumed that placing the bottom fiber in contact with the top fiber does not change this relationship.

After a TET measurement has been done on the top fiber to determine k_e and *dR/dT*, it can be placed in contact with the bottom sample. For this measurement, a Pt wire is used as the bottom sample, so that the thermal resistance of the bottom sample is small compared to the contact resistance.

6.4. Glass Fiber/Pt Wire Results

A glass fiber sample was mounted as described above and a TET measurement was done. The measured effective thermal diffusivity of the sample was 1.095×10^{-6} m^2/s. The effective thermal conductivity can then be calculated to be 1.60 W/mK. The steady state temperature rise and *dR/dT* can also be calculated. The experimental conditions and results of the TET measurement are summarized in Table 4. The data fitting is shown in Figure 19.

Table 4: Experimental conditions and results for glass fiber TET

Length:	1.08 mm
Heating Current:	150 μA
Resistance:	1070 Ω
Effective Thermal Diffusivity:	1.095×10^{-6} m^2/s
Effective Thermal Conductivity:	1.814 W/mK
Temp. Coefficient of Resistance:	0.6913 Ω/K

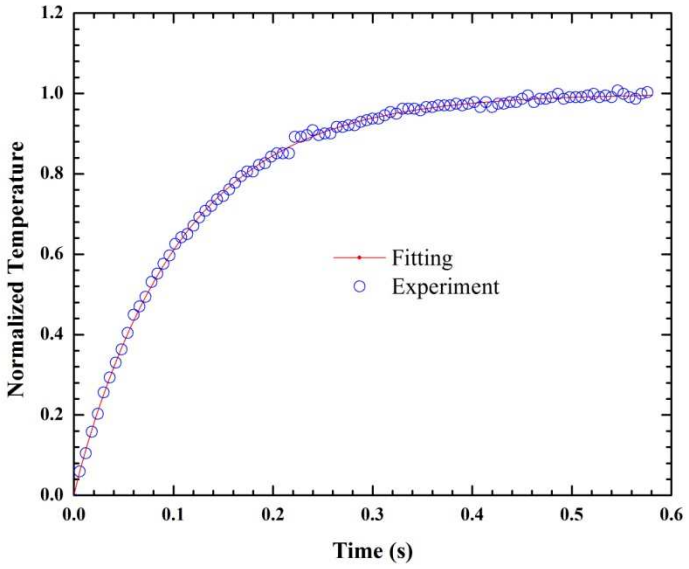

Figure 19: Data fitting for glass fiber TET

The glass fiber was put in contact with a Pt wire and a CTET measurement was done. The thermal contact resistance from the analytical steady state solution is 2.87×10^{7} K/W. The numerical transient solution gives a TCR of 2.94×10^{7} K/W. Again, the two results agree within 3%. The results of the CTET measurement are given in Table 5 and the data fitting is given in Figure 20. Figure 21 shows the effect that the thermal contact resistance has on the transient temperature rise of the sample.

Table 5: experimental conditions and results for glass fiber/Pt Wire CTET

Glass Fiber Length (mm):	1.08
Pt Wire Length (mm):	1.00
Heating Current (μA):	150
Analytical Rc (K/W):	2.871×10^{7}
Numerical Rc (K/W):	2.943×10^{7}

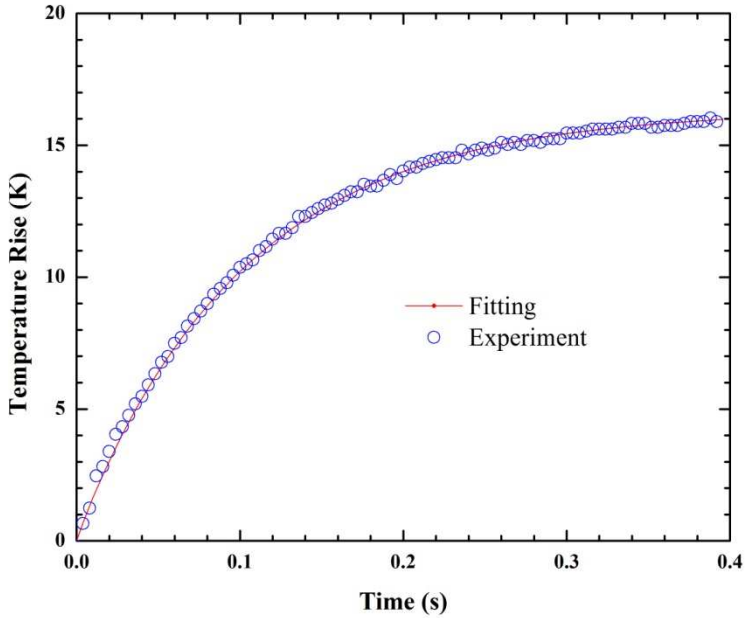

Figure 20: Data fitting for glass fiber on Pt CTET

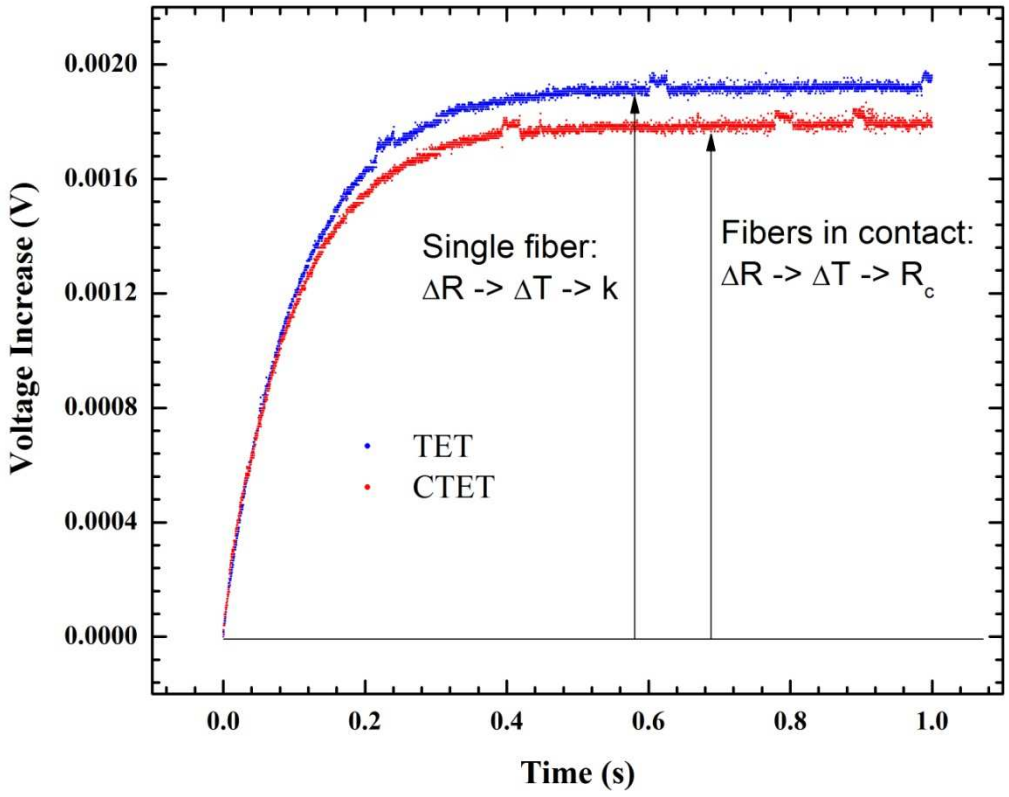

Figure 21: Comparison of TET and CTET measurements for glass fiber on Pt wire sample

A second glass fiber sample was mounted for additional TET and CTET measurements. This sample was shorter than then other sample, at 0.67 mm. Due to the shorter length of this sample, bringing the Pt wire into contact from the bottom was not feasible, so the Pt wire was brought into contact from the top. This means that the contact is between the gold coating on the glass fiber and the Pt wire. However, as the results of the measurements will show, this does not greatly change the value of the thermal contact resistance. The results of these measurements are given in Table 6. The data fittings for both the TET and CTET measurements are given in Appendix G.

Table 6: Experimental conditions and results for second glass fiber TET and CTET

Glass Fiber Length:	0.67 mm
Heating Current:	300 μA
Resistance:	920 Ω
Effective Thermal Diffusivity:	4.938×10^{-7} m^2/s
Effective Thermal Conductivity:	0.8177 W/mK
Temp. Coefficient of Resistance:	0.1033 Ω/K
Pt Wire Length:	1.00 mm
Steady State Temp. Increase:	81.5 K
Analytical Rc:	2.37×10^{7} K/W
Numerical Rc:	2.30×10^{7} K/W

Chapter 7. Discussion

The measurements taken using the CTET technique for both contact between Pt wires and contact between glass fiber and Pt wire give good results. The values obtained are reasonable and are in the range that would be expected. The excellent agreement between the steady state analytical and transient numerical solutions demonstrates the strength of the technique.

The thermal contact resistances obtained from the Pt wire measurements vary almost an order of magnitude. There seems to be a trend however, of increasing contact resistance with increasing heating current, which would mean a larger temperature rise. In general, the thermal conductivity of metals decreases as temperature increases due to increased electron-phonon scattering.[1] It is possible that there is also an enhanced phonon-phonon and electron-phonon scattering at the contact at higher temperatures, increasing the thermal contact resistance. Except for the measurements done at 30mA and 40mA, the analytical and numerical values agree within 3%. It may be interesting to note that the 50mA measurements were done on different days, while the 20mA measurement was the first measurement on that sample, and then the 30mA and 40mA were done immediately after. It may be that doing subsequent measurements affected the sample and is responsible for the disagreement.

The thermal contact resistance between the glass fiber and the Pt wire is about an order of magnitude higher than the TCR between Pt wires. This is expected because the thermal and acoustic properties of glass and Pt are very different. The glass fiber is an amorphous material and has a low thermal conductivity. The Pt wire is a metal, which has a much higher thermal conductivity and where the heat transfer is dominated by electrons. Another more likely reason for the higher TCR is the fact that the Pt wires have a larger diameter, therefore the actual

contact area between the fibers is most likely larger as well. For the measurement of the glass fiber and Pt wire, the steady state analytical and transient numerical solutions agree within 3%.

There are several ways that error could be introduced into the measurement of the TCR. One way is uncertainty in the length measurements of the fibers and wires. The estimated uncertainty in the sample length measurements is 1%. Another possible source of uncertainty is the location of the junction between the fibers. The derivation of the equations used in the data processing assumes that the fibers are in contact at their respective midpoints. However, upon further examination, it can be seen that if the contact is not at the midpoint, the temperature distribution may not be perfectly symmetric, but the average temperature of the wires will be the same. Thus, uncertainty in the placement of the contact does not add uncertainty to the measurement.

The largest source of possible variation between successive measurements is the contact pressure between the fibers. This was not controlled beyond manually turning the dial on the microstage and visually determining if the fibers were in contact. The bottom fiber was raised until the fibers were in contact, but not far enough to significantly bend the top fiber or change its resistance or dR/dT. The variability of the contact pressure between measurements may be a main reason for the variability of the measured TCR.

In the numerical calculation of the TCR for the Pt wire measurements, a value for the specific heat of Pt which is about 9% higher than the reference value was used. The reference value for Pt is 133 kJ/kgK,[26] while the value used in the calculations was 145 kJ/kgK. This is considered to be within the uncertainty of the measurement. A possible reason for this necessity is that the temperatures at the ends of the wire are not held at a constant temperature as assumed

in the theoretical calculations. The thermal capacitance of the electrodes may have an effect on the measurement.

One final issue to be addressed is the effect of thermal radiation on the measurement. For the glass fiber samples, radiation may have an important effect. The ratio of the amount of heat lost as thermal radiation to the amount of heat generated in the sample has been estimated to be approximately[47]

$$\frac{q_{rad}}{q_{gen}} \approx \frac{4\varepsilon\sigma L^2 T_0^2}{3kd}. \tag{36}$$

where ε is the surface emissivity of the sample, σ is the Stefan-Boltzmann constant (5.67 x 10^{-8} $Wm^{-2}K^{-4}$), L is the sample length, d is the diameter, T_o is the initial temperature, and k the thermal conductivity. By keeping the length of the glass fiber sample to around 1mm or less, this ratio becomes less than 10% and radiation introduces less uncertainty into the measurement. Even so, the effect of radiation heat loss can be seen in the difference between the two glass fiber measurements. The longer of the two glass fibers has an effective thermal diffusivity that is more than double that of the shorter glass fiber. This increase in effective thermal diffusivity is due to the increased radiation heat loss in the longer fiber. Additional TET measurements of different length glass fibers have shown that the effective diffusivity varies linearly with the fiber length squared. For the Pt wire samples, the high thermal conductivity and low emissivity of the sample ensures that radiation heat transfer is negligible even for longer samples.

Chapter 8. Conclusion

The work presented here has demonstrated several techniques for characterizing heat transfer in micro/nanoscale domains. Established one-dimensional techniques were used to determine the thermal properties of a variety of samples. Specifically, the photothermal method was used to measure the thermal conductivity of several thin film samples and the TET technique was used to measure the thermal diffusivity of several microscale wire and fiber samples.

Once the effective application of these one-dimensional methods was adequately demonstrated, a technique was developed to essentially characterize zero-dimensional heat transfer, or heat transfer in a single point. This was done by measuring the thermal contact resistance between two crossed microwires. Several crossed Pt wire samples were measured and found to have a thermal contact resistance on the order of 10^5-10^6 K/W. A glass fiber sample crossed with Pt wire was shown to have a thermal contact resistance on the order of 10^7 K/W. The agreement between samples, as well as the agreement between the steady state analytical and transient numerical solutions indicates the effectiveness of the technique.

This work is significant for two reasons. First, the concept of zero-dimensional heat transfer has not been addressed before in the context of a thermal contact resistance. Second, this technique could be useful for several different applications. Future studies using this technique could include measuring the thermal contact resistance between carbon nanotubes to better understand heat transfer in CNT composite materials. Also, this technique could be used to measure the TCR between cloth fibers to better predict the thermal behavior of textile materials.

Appendix A: Solution to Multilayer One-Dimensional Heat Transfer Equation

Adapted from Reference (15)

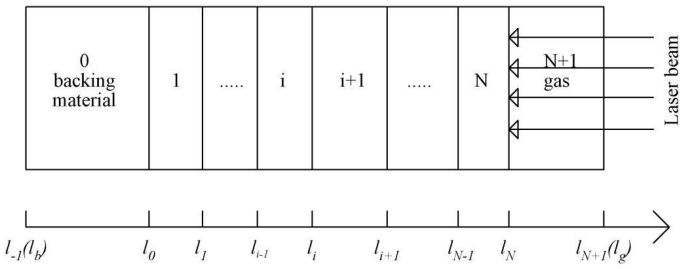

Figure A: N-layer sample for phothothermal/photoacoustic technique

Figure A shows a cross-sectional view of a multilayer sample under consideration. For a laser beam with energy flux $I = I_0(1 + \cos \omega t)/2$, the thermal diffusion equation for the i^{th} layer is

$$\frac{\partial^2 \theta_i}{\partial x^2} = \frac{1}{\alpha_i}\frac{\partial \theta_i}{\partial t} - \frac{\beta_i I_0}{2k_i}\exp\left(\sum_{m=i+1}^{N} -\beta_m L_m\right) e^{\beta_i (x-l_i)}\left(1 + e^{j\omega t}\right).$$

Here $\theta_i = T_i - T_{amb}$ for ambient temperature T_{amb}, α_i, k_i and β_i are the thermal diffusivity, thermal conductivity, and optical absorption of layer i, respectively, and $j = \sqrt{-1}$. The solution to this equation has three parts: an initial transient component $\theta_{i,t}$, a steady component $\bar{\theta}_{i,s}$, and a steady alternating component that comes from the modulated beam heat source $\tilde{\theta}_{i,s}$. Only $\tilde{\theta}_{i,s}$ needs to be evaluated. The general solution is

$$\tilde{\theta}_{i,s} = \left[A_i e^{\sigma_i (x-h_i)} + B_i e^{-\sigma_i (x-h_i)} - E_i e^{\beta_i (x-h_i)} \right] e^{j\omega t}$$

Here,

$$E_i = G_i / \left(\beta_i^2 - \sigma_i^2\right)$$

where

$$G_i = \frac{\beta_i I_0}{2k_i}\exp\left(-\sum_{m=i+1}^{N}\beta_m L_M\right) \quad for \quad i < N,$$

$$G_N = \frac{\beta_N I_0}{2k_N} \quad and \quad G_{N+1} = 0.$$

Also, $h_i = l_i$ for $i = 0, 1, \ldots, N$, $h_{N+1} = 0$ and $\sigma_i = (1+j)\sqrt{\omega/2\alpha}$. Assuming that the backing material (layer 0) and the gas layer (layer N+1) are thermally thick, the coefficients $A_{N+1} = B_0 = 0$. The other coefficients can be found by considering the conditions at the layer boundaries, where the heat flux is continuous, but the temperature is not due to thermal contact resistance:

$$k_i\frac{\partial\tilde{\theta}_{i,s}}{\partial x} - k_{i+1}\frac{\partial\tilde{\theta}_{i+1,s}}{\partial x} = 0$$
$$k_i\frac{\partial\tilde{\theta}_{i,s}}{\partial x} + \frac{1}{R_{i,i+1}}\left(\tilde{\theta}_{i,s} - \tilde{\theta}_{i+1,s}\right) = 0.$$

This leads to a matrix form of a recurrence formula for finding the coefficients:

$$\begin{bmatrix} A_i \\ B_i \end{bmatrix} = U_i\begin{bmatrix} A_{i+1} \\ B_{i+1} \end{bmatrix} + V_i\begin{bmatrix} E_i \\ E_{i+1} \end{bmatrix}.$$

where

$$U_i = \frac{1}{2}\begin{bmatrix} u_{11,i} & u_{12,i} \\ u_{21,i} & u_{22,i} \end{bmatrix};$$
$$V_i = \frac{1}{2}\begin{bmatrix} v_{11,i} & v_{12,i} \\ v_{21,i} & v_{22,i} \end{bmatrix};$$
$$u_{1n,i} = \left(1 \pm k_{i+1}\sigma_{i+1}/k_i\sigma_i \mp k_{i+1}\sigma_{i+1}R_{i,i+1}\right)\exp\left[\mp\sigma_{i+1}\left(h_{i+1} - h_i\right)\right], \quad n = 1,2;$$
$$u_{2n,i} = \left(1 \mp k_{i+1}\sigma_{i+1}/k_i\sigma_i \mp k_{i+1}\sigma_{i+1}R_{i,i+1}\right)\exp\left[\mp\sigma_{i+1}\left(h_{i+1} - h_i\right)\right], \quad n = 1,2;$$
$$v_{n1,i} = 1 \pm \beta_i/\sigma_i, n = 1,2;$$
$$v_{n1,i} = \left(-1 \mp k_{i+1}\beta_{i+1}/k_i\sigma_i + k_{i+1}\beta_{i+1}R_{i+1}\right)\exp\left[-\beta_{i+1}\left(h_{i+1} - h_i\right)\right], \quad n = 1,2.$$

The physical interpretation of U_i is the heat transmission matrix between layer (i+1) and layer i. The physical interpretation of V_i is the absorption matrix of light from the incident laser beam.

Appendix B: Solution to One-Dimensional Heat Transfer Equation for TET

Adapted from Reference (17)

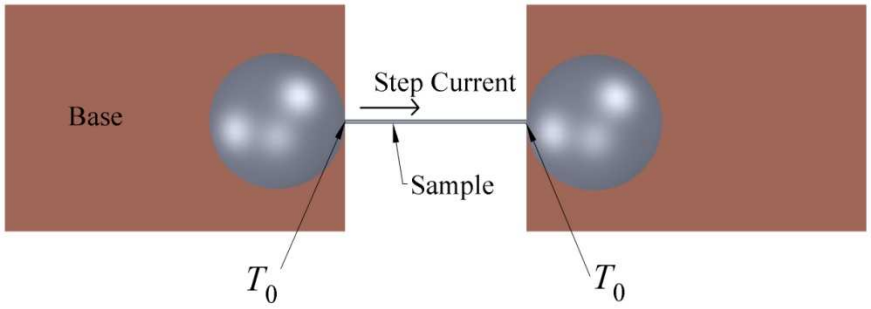

Figure B: Principle of TET experiment

Figure B shows the geometry under consideration. For one-dimensional heat transfer with heat generation, the governing equation is

$$\frac{\rho c_p \partial T}{\partial t} = k\frac{\partial^2 T}{\partial x^2} + q_0$$

for thermal conductivity k, density ρ, and specific heat c_p. q_0 is the electrical heating power per unit volume, which is assumed to be constant as $q_0 = \frac{I^2 R_0}{LA}$, where R_0 is the initial resistance of the sample, L is the sample length, and A is the cross sectional area. The initial condition and boundary conditions are

$$\begin{gathered} T(x, t=0) = T_0 \\ T(x=0, t) = T(x=L, t) = T_0 \end{gathered}.$$

This PDE can be solved using the Green's function integral method. The Green's function for this equation is

$$G_{x11}(x,t\,|\,x',\tau)=\frac{2}{L}\sum_{m=1}^{\infty}1-\exp\left[-m^2\pi^2\alpha(1-\tau)/L^2\right]\sin\left(m\pi\frac{x}{L}\right)\sin\left(m\pi\frac{x'}{L}\right).$$

The temperature distribution can be found to be $T(x,t)=T_0+\frac{\alpha}{k}\int_{\tau=0}^{t}\int_{x'=0}^{L}q_0G_{x11}dx'd\tau$. The temperature averaged along the length of the wire is

$$T(t)=\frac{1}{L}\int_{x=0}^{L}T(x,t)dx=T_0\frac{8q_0L^2}{k\pi^4}\sum_{m=1}^{\infty}\frac{1-\exp\left[-(2m-1)^2\pi^2\alpha t/L^2\right]}{(2m-1)^4}.$$

The steady state temperature can be found by taking the limit as time goes to infinity:

$$T(t\to\infty)=T_0+\frac{q_0L^2}{12k}.$$

The normalized temperature is defined as

$$T^*(t)=\frac{T(t)-T_0}{T(t\to\infty)-T_0}.$$

This can be written as

$$T^*=\frac{96}{\pi^4}\sum_{m=1}^{\infty}\frac{1-\exp\left[-(2m-1)^2\pi^2\alpha t/L^2\right]}{(2m-1)^4}.$$

Appendix C: Properties used in data processing for SiC photothermal measurement

Chromium:	Thermal Conductivity (W/mK):	93.7
	Specific Heat (J/kgK)	449
	Density (kg/m^3)	7160
	Thickness (nm)	80
Silicon:	Thermal Conductivity (W/mK):	148
	Specific Heat (J/kgK):	712
	Density (kg/m^3):	2330
SiC:	Specific Heat (J/kgK):	690
	Density (kg/m^3)	3160
	Thickness (μm)	2.5

Appendix D: Properties used in data processing for PBL-Al photothermal measurements

Gold:	Thermal Conductivity (W/mK):	317
	Specific Heat (J/kgK)	129
	Density (kg/m^3)	19300
	Thickness (nm)	100
Silicon:	Thermal Conductivity (W/mK):	148
	Specific Heat (J/kgK):	712
	Density (kg/m^3):	2330
PBL-Al:	Specific Heat (J/kgK):	880
	Thickness (μm)	6.0

Appendix E: Properties used in data processing for Carbon film photothermal measurements

Gold:	Thermal Conductivity (W/mK):	317
	Specific Heat (J/kgK)	129
	Density (kg/m^3)	19300
	Thickness (nm)	100
LTCC:	Thermal Conductivity (W/mK):	6.6
	Specific Heat (J/kgK):	756
	Density (kg/m^3):	2958
Carbon Film:	Specific Heat (J/kgK):	509
	Thickness-P3 (µm)	4.0
	Thickness-P7 (µm)	7.0

Appendix F: Data fittings for Pt wire CTET measurements

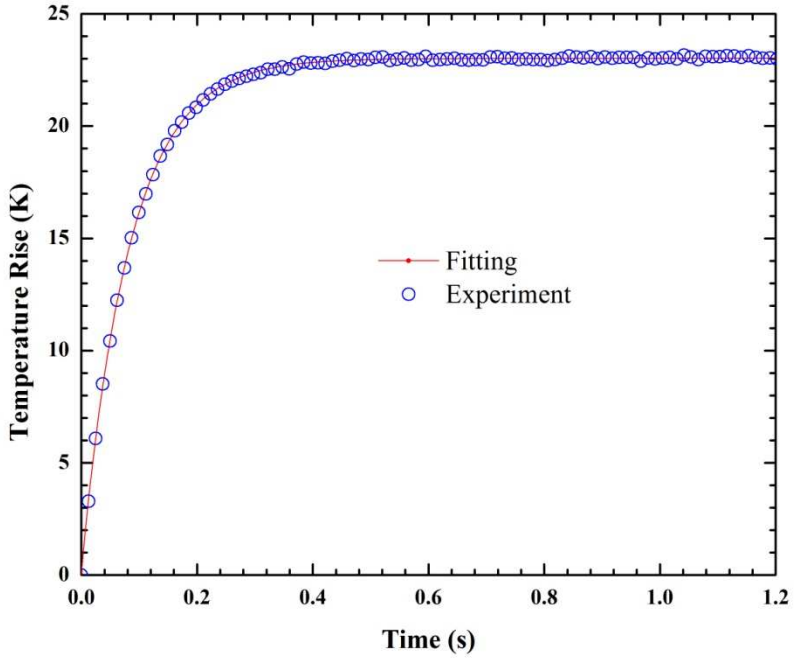

Figure F-1: Data fitting for Pt wire CTET - 50mA first measurement

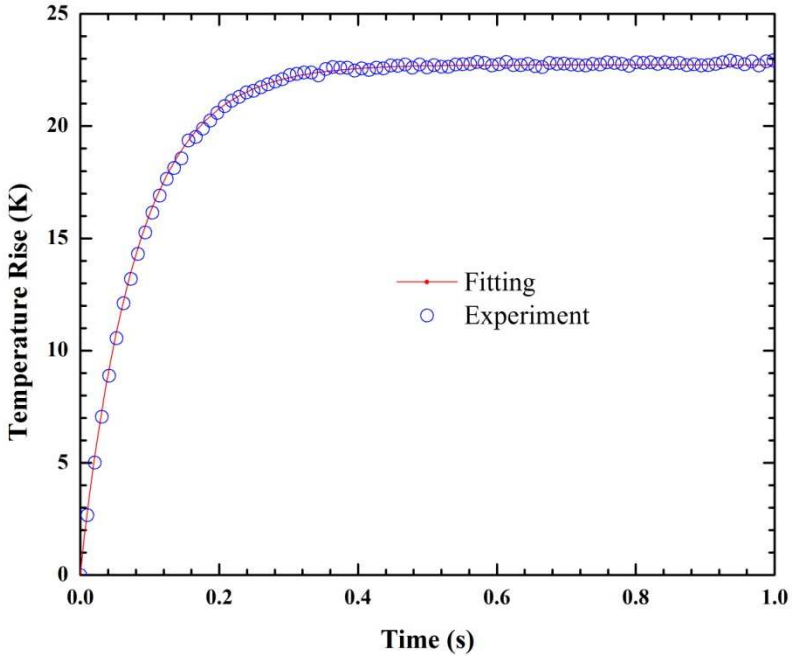

Figure F-2: Data fitting for Pt wire CTET - 50mA second measurement

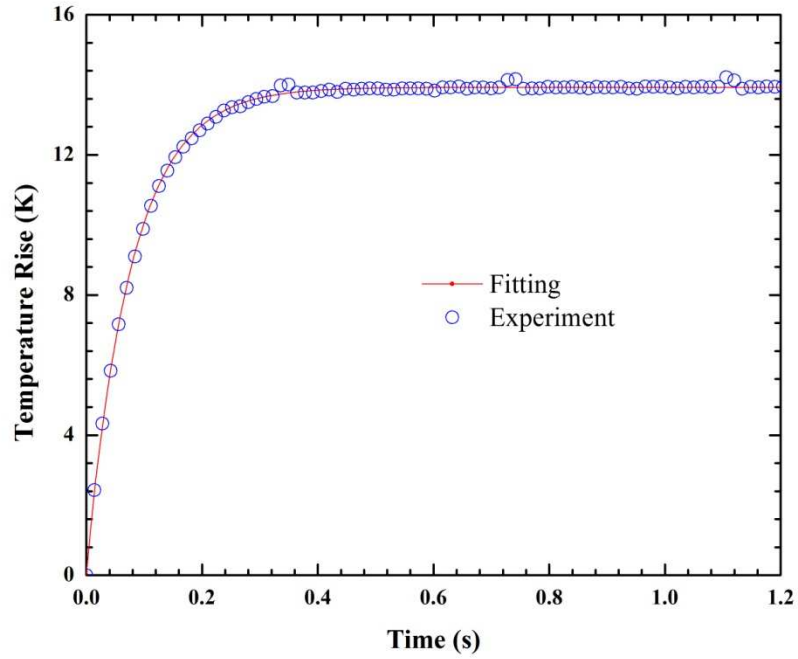

Figure F-3: Data fitting for Pt wire CTET - 40mA

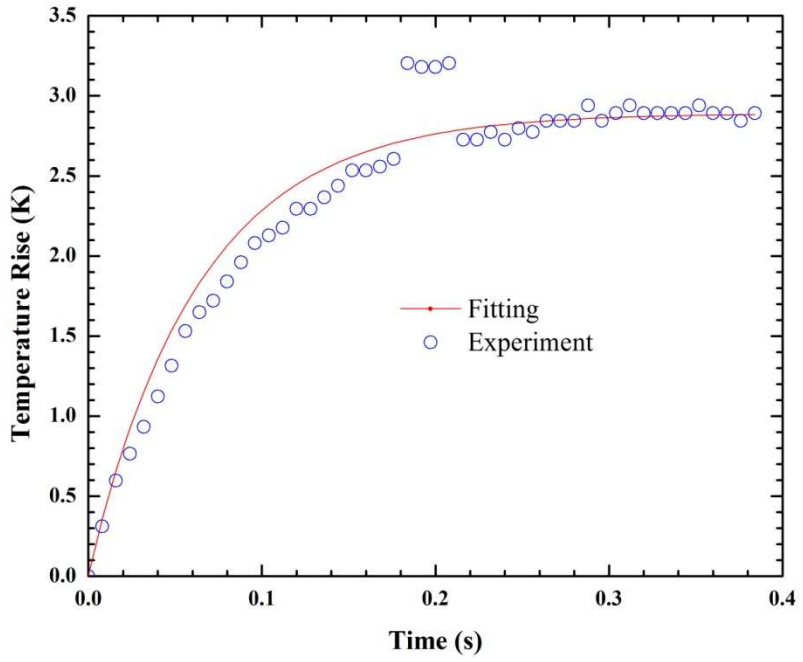

Figure F-4: Data fitting for Pt wire CTET - 30mA

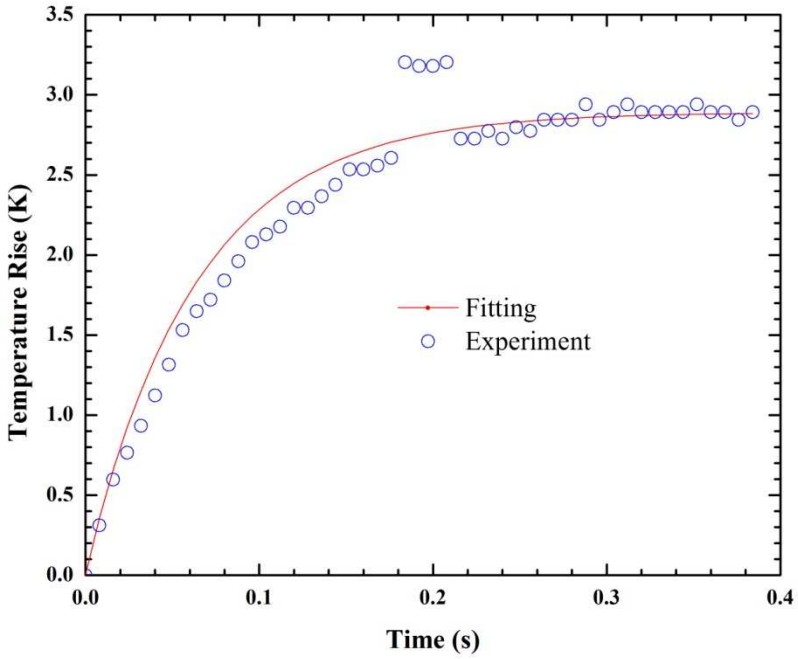

Figure F-5: Data fitting for Pt wire CTET - 20 mA

Appendix G: Data Fitting for 0.67mm Glass Fiber on Pt wire TET and CTET measurements

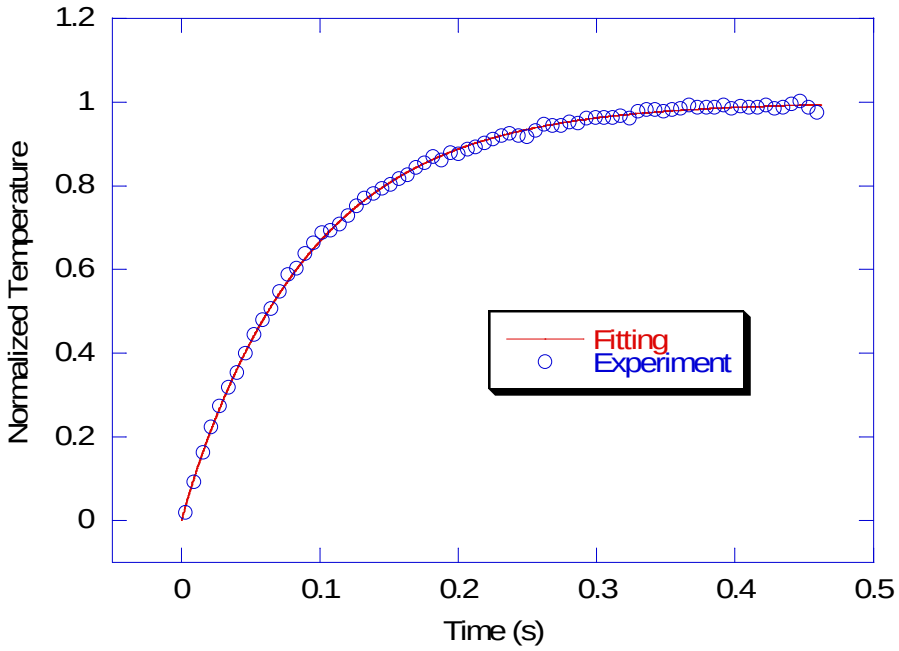

Figure G-1: Fitting results for TET measurement of 0.67mm glass fiber sample

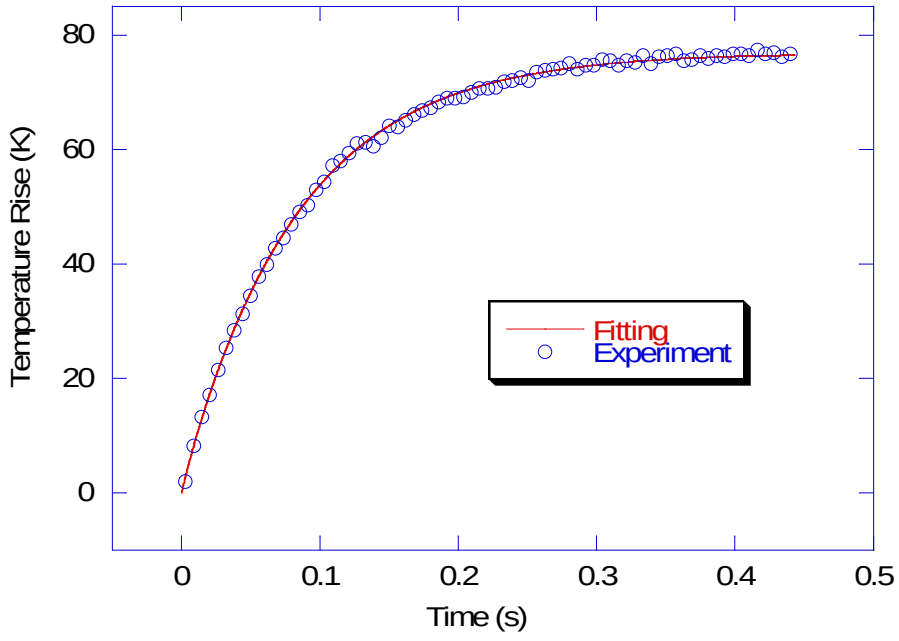

Figure G-2: Fitting Results for CTET measurement of 0.67 glass fiber sample on Pt wire

References

[1]Z. M. Zhang, *Nano/Microscale Heat Transfer* (McGraw-Hill, New York, 2007).

[2]C. B. Sobham and G. B. Peterson, *Microscale and Nanoscale Heat Transfer* (CRC Press, Boca Raton, 2008).

[3]D. G. Cahill, Rev. Sci. Instrum. **61,** 802-808 (1990).

[4]J. Hou, X. Wang, P. Vellelacheruvu, J. Guo, C. Liu, and H.-M. Cheng, Journal of Applied Physics **100,** 124314 (2006).

[5]Y. S. Ju and K. E. Goodson, *Microscale Heat Conduction in Integrated Circuits and Their Constituent Films* (Kluwer Academic Publishers, Norwell, 1999).

[6]J. H. Kim, A. Feldman, and D. Novotny, Journal of Applied Physics **86,** 3959-3963 (1999).

[7]H. Wang and M. Sen, International Journal of Heat and Mass Transfer **52,** 2102-2109 (2008).

[8]T. Tong and A. Majumdar, Rev. Sci. Instrum. **77,** 104902 (2006).

[9]A. Jain and K. E. Goodson, ASME Journal of Heat Transfer **130,** 102402 (2008).

[10]A. Jacquot, F. Vollmer, B. Bayer, M. Jaegle, D. G. Ebling, and H. Bottner, Journal of Electronic Materials **39,** 1621-1626 (2010).

[11]L. Lu, W. Yi, and D. L. Zhang, Rev. Sci. Instrum. **72,** 2996-3003 (2001).

[12]T.-Y. Choi, D. Poulikakos, J. Tharian, and U. Sennhauser, Nano Letters **6,** 1589-1593 (2006).

[13]F. A. McDonald, Can. J. Phys. **64,** 1023-1029 (1986).

[14]W. A. McGahan and K. D. Cole, Journal of Applied Physics **72,** 1362-1373 (1992).

[15]H. Hu, X. Wang, and X. Xu, Journal of Applied Physics **86,** 3953-3958 (1999).

[16]T. Wang, X. Wang, Y. Zhang, L. Liu, L. Xu, Y. Liu, L. Zhang, Z. Luo, and K. Cen, Journal of Applied Physics **104,** 013528 (2008).

[17]J. Guo, X. Wang, and T. Wang, Journal of Applied Physics **101,** 063537 (2007).

[18]X. Feng, X. Chen, and X. Wang, Acta Materialia **59,** 1934-1944 (2011).

[19]X. Feng and X. Wang, Thin Solid Films **519,** 5700-5705 (2011).

[20]X. Huang, G. Liu, and X. Wang, Advanced Materials **communications** (2012).

[21]J. Hou, X. Wang, and J. Guo, J. Phys. D: Appl. Phys. **39,** 3362-3370 (2006).

[22]T. Wang, X. Wang, J. Guo, X. Lou, and K. Cen, Appl. Phys. A **87,** 599-605 (2007).

[23]J. Guo, X. Wang, D. B. Geohegan, G. Eres, and C. Vincent, Journal of Applied Physics **103,** 113505 (2008).

[24]J. Guo, X. Wang, D. B. Geohegan, and G. Eres, Functional Materials Letters **1,** 71-76 (2008).

[25]Y. Yue, G. Eres, X. Wang, and L. Guo, Appl. Phys. A **97,** 19-23 (2009).

[26]M. M. Yovanovich, IEEE Transactions on Components and Packaging Technologies **28,** 182-206 (2005).

[27]E. T. Swartz and R. O. Pohl, Review of Modern Physics **61,** 605-668 (1989).

[28]S. Shenogin, L. Xue, R. Ozisik, P. Keblinski, and D. G. Cahill, Journal of Applied Physics **95,** 8136-8144 (2004).

[29]S. T. Huxtable, D. G. Cahill, S. Shenogin, L. Xue, R. Ozisik, P. Barone, M. Usrey, M. S. Strano, G. Siddons, M. Shim, and P. Keblinksi, Naure Materials **2,** 731-734 (2003).

[30]H. Zhong and J. R. Lukes, Physical Review B **74,** 125403 (2006).

[31]R. S. Prasher, X. J. Hu, Y. Chalopin, N. Mingo, K. Lofgreen, S. Volz, F. Cleri, and P. Keblinski, Physical Review Letters **102,** 105901 (2009).

[32]J. Wang, K. Bi, and Y. Chen, Key Engineering Materials **483,** 663-667 (2011).

[33]J. Yang, S. Waltermire, Y. Chen, A. A. Zinn, T. T. Xu, and D. Li, Applied Physics Letters **96,** 023109 (2010).

[34]L. Guo, J. Wang, Z. Lin, S. Gacek, and X. Wang, Journal of Applied Physics **106,** 123526 (2009).

[35]X. Zhang, S. Fujiwara, and M. Fujii, International Journal of Thermophysics **21,** 965-980 (2000).

[36]J. L. Wang, M. Gu, X. Zhang, and Y. Song, J. Phys. D: Appl. Phys. **42,** 105502 (2009).

[37]J. Wang, M. Gu, X. Zhang, and G. Wu, Rev. Sci. Instrum. **80,** 076107 (2009).

[38]J. Wang, B. Song, M. Gu, and X. Zhang, International Journal of Heat and Mass Transfer **53,** 5350-5354 (2010).

[39]F. P. Incropera, D. P. Dewitt, T. L. Bergman, and A. S. Lavine, *Fundamentals of Heat and Mass Transfer*, 6th ed. (John Wiley & Sons, Hoboken, 2007).

[40]F. Macedo and J. A. Ferreira, Rev. Sci. Instrum. **74,** 828-830 (2003).

[41]R. Postle, Fire Safety Journal **4,** 83-89 (1981).

[42]M. I. Ismail, A. S. A. Ammar, and M. El-Okeily, Appl. Math. Modelling **12,** 434-440 (1988).

[43]X. J. Ran, Q. Y. Zhu, and Y. Li, International Journal of Heat and Mass Transfer **54,** 3575-3586 (2011).

[44]J. C. Tannehill, D. A. Anderson, and R. H.Pletcher, *Computational Fluid Mechanics and Heat Transfer*, 2nd ed. (Taylor & Francis, Philadelphia, 1997).

[45]H. D. Young and R. A. Freedman, *University Physics*, 11th ed. (Pearson Addison Wesley, San Francisco, 2004).

[46]S. Kakac and H. Liu, *Heat Exchangers; Selection, Rating and Thermal Design*, 2nd ed. (CRC Press, Boca Raton, 2002).

[47]X. Huang, J. Wang, G. Eres, and X. Wang, Carbon **49,** 1680-1691 (2011).